Doctoral Dissertation (Shinshu University)

Development and applications of high-performance passive cooling nanocomposite films for energy consumption saving

March 2021

Cui Lina

Department of Science and Technology

Graduate School of Medicine, Science and Technology

Contents

Abbreviations

UV	ultraviolet
Vis	visible
nIR	near infrared
mid-IR	mid-infrared
SV	specific volume
ΔT	temperature reduction
PI	polyimide
NP	nanoparticle
ZnO	zinc oxide
LDPE	low density polyethylene
SEM	scanning electron microscope
UV–Vis–nIR	ultraviolet–visible–near infrared
FTIR	Fourier transform infrared
RH	relative humidity
DSC	defferential scanning calorimeter
ZnO	zinc oxide
LDPE	low density polyethelene
4% film	film with a particle concentration of 4%
5% film	film with a particle concentration of 5%
6% film	film with a particle concentration of 6%

Abstract

Energy expenditure in buildings and transportation is about 63% of global energy consumption. It is reported that temperature regulation for buildings and automobiles takes 60% and 23 to 41% of their total energy expenditure, respectively, leading to excessive greenhouse gas emissions. One of the strategies, which has attracted plenty of attentions in recent years, for cooling space without any kind of energy input to a special cooling system is to use passive cooling films. In this dissertation, flexible spectrum selective transparent passive cooling films were developed using zinc oxide (ZnO) nanoparticles (NPs) dispersed in low-density polyethylene (LDPE). Their basic properties (such as mechanical, thermal, and optical characters) and cooling performance were systematically studied in different applicating conditions with variation in the intensity of solar radiation, the ratio of window area to enclosed cooling volume, and shielding ratio of visible (Vis) light.

First, flexible spectrum selective transparent ultraviolet (UV)-shielding films were fabricated by casting method, which uniformly dispersed pristine ZnO NPs in LDPE. The critical conditions for film fabrication, such as casting temperature, LDPE concentration in the solution, dissolution time, NP concentration, and post hot press cooling processes, are systematically studied. Ideal films were successfully fabricated with well dispersed NPs and could completely shield UV light while allowing high transmissivity for the Vis and infrared (IR) photons. The basic property characters of membrane like dispersion of NPs in the films, transmissivity, thermal property, and tensile strength were tested.

Passive cooling performances of spectrum selective films were evaluated with a self-made passive cooling test system, designed with the consideration of actual engineering application.

For detecting the influence of the intensity of solar radiation, the cooling performances monitored for 24 h showed that the air temperature inside of the testing boxes were raised as the intensity of solar irradiance increased in daytime. Under a fixed ratio of volume versus window area of test boxes, the 6%-ZnO film had the largest temperature reduction (ΔT) compared with the temperature of the control box reaching 8.84 ºC, with a corresponding cooling power of 361 W/m^2. It was also observed that the films had cooling effect at night, reaching 1.41 ºC at mid-night, compared with the temperature of the control box too.

The cooling performance of films was influenced by volumes per unit window area or specific volume (SV). Like cars, commercial offices and common residentials, which has different SV, are constructed with windows for daylighting and good scene. The testing results showed that temperature reduction compared with the control, ΔT (up to 14.95 ºC), of the films decline exponentially initially and then levels-off as SV increases. An empirical model is proposed for the relationship between ΔT and SV according to the actual engineering applications, which guides for practical end uses. Furthermore, SVs of passenger cars and office buildings are found to be located within the most sensitive range of the ΔT-SV curve of our films.

And the regression equation of cooling performance with different shielding ratio of Vis showed liner relationships. Data showed that the better Vis-shielding effect of the films, the better cooling effect of films performed.

Based on these results, transparent passive-cooling films can almost completely shield UV light and partially shield Vis light while allowing most mid-IR light to pass,

due mainly to light scattering. The films also can lower the temperature by 4.34–14.95 °C. Therefore, our cooling film can be highly beneficial for energy saving in passenger cars and large window commercial offices. Meanwhile, even for regular residential buildings and open spaces, our film could potentially lower the temperature by about 4 ºC at midday, significantly reducing cooling energy consumption.

Chapter 1 General introduction

Chapter 1 General introduction

1.1 Energy expenditure for space cooling made climate change

The two largest energy consumption sectors are buildings and transportation taking about 63% [1, 2] of global energy consumption. As buildings and automobiles exposed directly under solar radiation, the cabins of buildings and automobiles gain heat from solar spectrum which pass through the windows equipped for daylighting demands. For cooling cabin spaces, more and more air conditionings are utilized, which consumes more energy, especially in summer. It is reported that energy consumption on temperature regulation for buildings and automobiles, which gain through window systems, consumes 60% [2, 3] and 23 to 41% [4, 5] of global energy expenditure, respectively, hence leading to excessive greenhouse gas emissions, like carbon dioxide (CO_2) [6-10]. In recent decades, the design trend of car [11] and commercial architecture is going to combine increasingly more and larger windows for lighting and good scene [12]. Large office buildings and skyscrapers are often entirely enveloped with glasses, which can receive plenty of heat gaining from solar irradiance, a part of thermal radiation wavelength rang.

Thermal radiation wavelength range is in region of 100 nm to 1000 μm [13]. The sun closely matches a black body radiator at about 5,800 K [13]. And the wavelength range of solar spectrum, which irradiates from solar and finally reaches on the earth surface, is

in range of 200 nm to 2.5 μm. Simultaneously, the solar photons carry higher energy to earth surface and heat items and living things which are radiated on. Solar photons involve ultraviolet (UV) light, visible (Vis) light, and near inferred (IR) light. It is reported that if a vehicle is exposed directly under solar radiation without any shielding in summer, the air temperature of cabin especially near the windshield could reach up to 80 ºC [14-16] in twenty minutes. Which gradually leads to larger and larger demanding of temperature regulation systems in our daily life, especially in summer. Hence plenty of research works have been done in cooling spaces by scientists all over the world. Chart a in **Fig. 1-1** showed the over period from 1975 to 2020, the technology innovation of automotive has been applied to vehicle design with different emphasis aspect on vehicle weight, power, CO_2 emissions, and fuel economy [17]. On the other hand, energy consumption on space heating and cooling are the dominant of that for both residential and commercial energy consumption. They contribute to 12.3% of total U.S. energy consumption. Reducing the demand for indoor temperature regulation will have substantial impact on global energy consumption **Fig. 1-1**. b [18].

Reducing the energy needs for temperature regulation of spaces of cabins or buildings will have substantial impact on global energy consumption. Although it was reported from the annual reports that the conventional approaches have been focusing on improving building insulation, enabling smart temperature control, and improving the energy efficiency of vehicle industries and electrical appliances [17-19]. But up to now, running the air conditioning also requires higher energy consumption even though the energy efficiency were enhanced greatly than before [20]. Some new approaches have been attempted in recent years, one of them is to develop a named passive or radiative cooling materials, which have the cooling function without any kind of energy input [21, 22], for both indoor and outdoor spaces. And it is a good promotion for sustainable

society development.

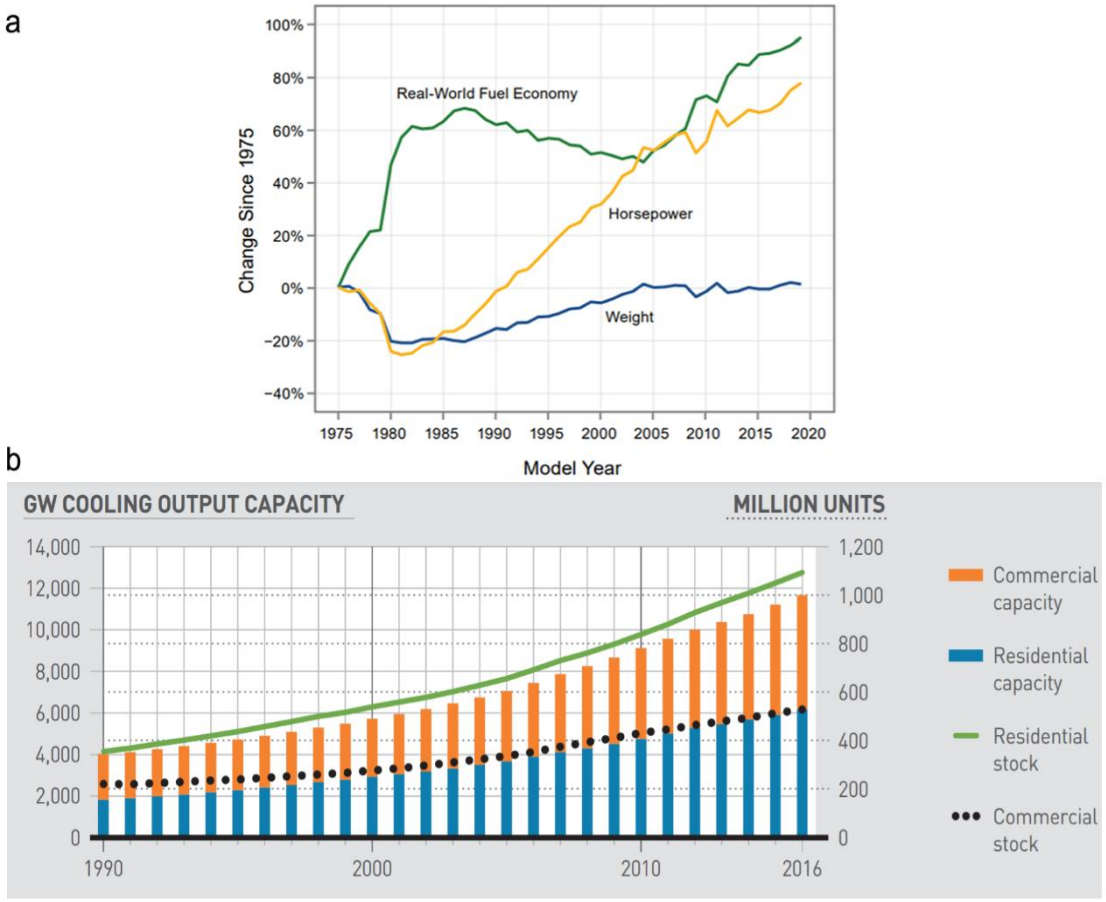

Fig. 1-1. a. Estimated Real-World Fuel Economy, Horsepower, and Weight Since Model Year 1975 (Sourced from The 2019 Environmental Protection Agency Automotive Trends Report [17]); b. worldwide stock and capacity of air-conditioning units by sectors, particularly to households, continue to grow briskly, enlarge the global cooling capacity (obtained from International Energy Agency Energy Conservation in Buildings and Community annual report 2018 [18]).

1.2 Passive cooling materials

Passive cooling is often achieved by blocking solar irradiance or highly transmitting mid-IR [22-26], which wavelength is longer than solar spectrum. So far, most of reported materials are opaque, most of which not only could totally shield solar irradiance (200 nm to 2.5μm), but also could make the IR especially for electromagnetic wave belonging to the atmosphere window (8μm and13μm) pass through. And Vall et al. gave an over review of the radiative cooling technology. They reported that the radiative cooling has been widely studied since 20th century, but the research is scattered all over the literature, the works were classified in: (1) radiative cooling background, (2) selective radiative cooling, (3) theoretical approach and numerical simulations, and (4) radiative cooling prototypes [27]. Thus far, however, almost all these radiative cooling materials are made of inorganic materials which are either opaque and/or involve complicated manufacturing processes and application mechanisms.

Radiative or passive cooling materials were developed broadly in construction field for reduction the energy consumption of spaces cooling. This kind materials can dramatically reduce the energy consumption since they are renewable and require low energy for their operation. Radiant cooling floor has the potential to improve indoor thermal comfort and energy efficiency as well as floor heating [28-30]. And some others focused on radiative construction materials too, like Li et al. reported on a radiative wood for cooling the building spaces [31]. And Raman et al. [23] and Hamdan et al. [32] reported their radiative roof materials. Al-Obaidi et al. gave an over review on other passive cooling or radiative roof materials for building space cooling [33].

And the flexible opaque materials were fabricated by some scientists [24, 34]. Xiang et al. [35] made a film with inorganic particles mixed in acrylonitrile-styrene-acrylate and found that the film was able to reduce temperature by 10°C due to reflection of solar radiation by the organic particles, and the films were opaque and would be easily scratched and gradually losing the cooling function. Li et al. fabricated opaque textile for outdoor personal cooling by shielding UV and visible lights [31].Some researchers work on the spectrum selective transparent passive cooling materials too. Most of these materials were nano composites. Little has been reported about translucent or transparent cooling films made of nanoparticles (NPs) and polymers. Fan et al. reported a 4.6 °C reduction using a translucent radiative cooling film made from fluorinated polyimide (PI) coated with SiO_2 microspheres and a silver layer [36]. However, PI films are not generally suitable for cost sensitive automobiles and office buildings.

In some circumstance situation, we need some functional materials combined with passive cooling and daylighting demands. So as to shield parts of solar radiation and make partial of solar photons pass through to satisfy the lighting demand. For developing these kinds of materials, we would like tailor the high-energy photons of solar spectrum. UV and Vis photons are serial of shorter wavelength spectrum carrying higher energy [37], which reach the terrestrial surface more than before because of the increased ozone depletion as indicated by Yoo et al. [38] and Xie et al. [39]. The UV photons can not only cause serious injuries to the skin which might eventually result in skin cancer Hacker et al. reported in literature [40], but also provide radiative heat which may cause consuming plenty of energy to regular the temperature of space[20]. And UV light is harmful to electrical facilities too, as Liu et al. described that the efficiency of electrical devices can be decreased close to 50% after a short exposure to the UV light [41]. More

and more attention has been paid for shielding UV photons recently years. Feng et al. [42] and Li et al. [43] fabricated transparent UV-shielding composites using cellulose which are hard for large scale production. Han et al. [44] reported they used 60 nm particle dispersing into polymer, and finally the particle were dispersed at about 600 nm in their samples, and the complete UV-shielding performance would appear when the NP concentration was higher than 7%, which would influence the visible light transparent. And Wang et al. [45] fabricated similar functional materials by mixing inorganic NPs with polymers, which also had a high NP concentration about 0.5 mol/ml. And the UV-shielding materials also can be a good candidate for passive cooling. Gamage et al. have shown that UV-shielding and visible transparent nanocellulose papers, of which the strength might be lower, might be a good candidate for passive cooling to save energy consumption [46]. More and more passive cooling or radiative materials were developed by nano fillers, named as nanocomposites.

1.3 Nano composite passive cooling materials

Nanotechnology gradually attracts the interests of scientists and engineers to develop new functional materials in recent 2 to 3 decades [47]. NPs are popularly utilized for promoting and functionalizing the property of polymeric materials in nanocomposites field [48]. Some literatures reported on passive cooling functional nano composites [49-51]. Especially the use of organic-inorganic materials is a popular way to prepare the flexible composites. In fact, the biggest challenge is how to uniformly disperse the NPs into inorganic materials, as polymers. It is difficult to dissolve the polyolefin in a large content to uniformly disperse NPs in its solution, as which have a relatively high molten viscosity, and suppressing the NP agglomeration. As the compatibility of NPs with most of polymers is often quite poor due to the difference in the properties of the two sorts of materials. Polyolefins exhibit low surface free energy, whereas NPs exhibit high surface energy, which may result in the agglomeration of NPs when the NPs are mixed with organic solvent and polyolefins. Thus, if there is serious NP agglomeration in composites, the functions of inorganic-organic composites would be hindered.

In order to improve the compatibility between NPs and polymers, surface treatments have been applied to modify the surface properties of NPs [52]. However, these treatments have the potential to induce adverse effects on the catalytic, optical, or magnetic properties of the surface-treated NPs. This may greatly influence the intended performance of the composites [49, 53]. El-Naggar and coworkers employed the core/shell structure to improve the agglomeration of ZnO NPs; however, the

characteristic absorption peaks of the NPs were shielded [54]. In addition, Hong et al. [55] reported reduced catalytic activity of coated ZnO NPs. In other literatures, similar observations have also been reported [56, 57].

Therefore, direct doping virgin NPs into the polymer could be preferable if one could achieve uniform dispersion of the NPs in the polymer when optimal mixing strategies could be adopted. In recent decades, various approaches have been attempted for the dispersion of NPs in polymers, including solution dispersion, mechanical blending, and *in situ* polymerization with NPs with their own advantages and disadvantages [58-60]. Mechanical blending is relatively simple but often suffers serious NP agglomeration when mixed into a highly viscose molten polymer [61-63]. *In situ* polymerization is highly selective for the polymer type that may be used as a matrix [64-66]. Solution methods are relatively easy to conduct an even dispersion of NPs in polymers, especially those without a melting temperature or with a high molten viscosity [67-69]. Polyolefins are synthesized *via* addition polymerization and thus have a relatively high degree of polymerization, which results in high molten viscosity [70]. Moreover, they are hard to dissolve in a solution without high temperature and long durations due to the saturated chemical structures, thus leading to poor affiliation with most of the organic solvents.

1.4 Purpose of this research

Since there are plenty of research works were involved in developing new materials, new methods to save energy consumption. Therefore, our research strategy was focused on developing passive cooling nanocomposites for space cooling without any kind of energy input. In this dissertation, a kind of flexible spectrum selective transparent films were developed, and their basic properties were investigated. Different films and different applicating conditions were selected to detect the cooling performances in detail, like the intensity of solar radiation, the ratio of space's window area and its volume or specific volume (SV), and shielding ratio of Vis light, to guide the engineering applications.

In chapter 1, the general energy expenditure of world was introduced, and the increasing demands of energy saving materials were gradually developed in corresponding scientific research fields. And the development of passive cooling material was introduced too. In nowadays the nano composite materials provided a sort of functions, especially in developing new passive cooling materials.

In chapter 2, a systemic experiment was designed to develop a kind of transparent flexible film with the function of passive cooling. Under the guidance of passive cooling material function, two raw materials of zinc oxide (ZnO) NPs [71] and low-density polyethylene (LDPE) [72] were selected to prepare the passive cooling materials. And according to the light scattering theories of Rayleigh or Mie, the particle sizes were calculated [73] and finally developed the transparent VU-shielding films. According to

the Gibbs-Helmholtz theory of polyolefin dissolving [70], we designed and carried out a systematic study to confirm fabricating and evaluating our ideal materials. A systematic experiment was conducted to determine the optimal casting temperature, LDPE concentration, and dissolution time for obtaining uniform dispersion of inorganic NPs in LDPE solution.

In chapter 3, the conditions for fabricating flexible spectrum selective transparent materials (ZnO/LDPE) were confirmed and the basic properties of which were detected. Polyolefins are synthesized *via* addition polymerization and thus have a relatively higher degree of polymerization, which also results in high molten viscosity [74]. Moreover, they are hard to dissolve in a solution without high temperature and long durations due to the saturated chemical structures, thus leading to poor affiliation with most of the organic solvents. This ZnO/LDPE composite films exhibited spectrum selective properties for shielding UV and diminished the transmittance of visible light and thus could be potentially used as passive cooling materials for the purpose of energy saving. Therefore, the basic properties of membranes as surfaces morphology, elemental analysis mapping, dispersion of NPs in the films, transmissivity, thermal property, and tensile strength were evaluated.

In chapter 4, the passive cooling performances of flexible spectrum selective transparent films were evaluated with a self-made temperature monitoring test system, designed with the consideration of actual engineering applications, which combined with temperature sensors, solar irradiance monitor, data loge, sealed boxes (which designed to minimize the heat transfer through conduction, convection, and secondary radiation from outside in and inside out), and humidity monitor. The influence factors of cooling performance like the intensity of incident light, SV, and shielding ratio of Vis region were detected.

The passive cooling performance of fabricated material was significant. The air temperatures inside of testing boxes, which window were either bare or covered with different film, showed that it would be raised as intensity of solar irradiation increases in daytime. Combining with practical engineering application, the cooling performances of membranes were tested at different volumes per unit window area or specific volume (SV), Like cars, commercial offices and common but each have a different radial between the window area and volume of their selves. The relationship between ΔT and SV is more appropriate for consideration for passive cooling performance of our samples. The regression equation of cooling performance with different shielding ratio of Vis showed liner relationships. Data showed that the better Vis-shielding effect of the films, the better cooling effect of films performed.

References

[1] R. Ruparathna, K. Hewage, R. Sadiq, Improving the energy efficiency of the existing building stock: A critical review of commercial and institutional buildings, Renew. Sust. Energ. Rev. 53 (2016) 1032-1045. https://doi.10.1016/j.rser.2015.09.084.

[2] R. Tällberg, B.P. Jelle, R. Loonen, T. Gao, M. Hamdy, Comparison of the energy saving potential of adaptive and controllable smart windows: A state-of-the-art review and simulation studies of thermochromic, photochromic and electrochromic technologies, Sol. Energy Mater Sol. Cells 200 (2019) 109828-109858. https://doi.10.1016/j.solmat.2019.02.041.

[3] P.H. Shaikh, N.B.M. Nor, P. Nallagownden, I. Elamvazuthi, T. Ibrahim, A review on optimized control systems for building energy and comfort management of smart

sustainable buildings, Renew. Sust. Energ. Rev. 34 (2014) 409-429. https://doi.10.1016/j.rser.2014.03.027.

[4] G.J. Marshall, C.P. Mahony, M.J. Rhodes, S.R. Daniewicz, N. Tsolas, S.M. Thompson, Thermal management of vehicle cabins, external surfaces, and onboard electronics: An overview, Engineering 5(5) (2019) 954-969. https://doi.10.1016/j.eng.2019.02.009.

[5] N. Gure, M. Yilmaz, Alternative solution via car window filming implementation to combat global warming and resulted benefits around geographic Europe and the European Union, Int. J. Glob. Warm. 10(1-3) (2016) 263-290. https://doi.10.1504/ijgw.2016.077917.

[6] I.E. Agency, Energy and air pollution World Energy Outlook Specoial Report, https://webstore.iea.org/download/summary/343?fileName=English-WEO-Air-Pollution-ES.pdf, 2016 (accessed 3 July 2020).

[7] I.E. Agency, Energy in Buildings and Communities Annual Report https://www.iea-ebc.org/Data/Sites/1/media/docs/AR/ebc_annual_report_2018.pdf, 2018 (accessed 5 July 2020).

[8] N. Oreskes, The scientific consensus on climate change (vol 306, pg 1686, 2004), Science 307(5708) (2005) 355-355. https://doi.10.1126/science.1103618.

[9] G.R. Walther, E. Post, P. Convey, A. Menzel, C. Parmesan, T.J.C. Beebee, J.M. Fromentin, O. Hoegh-Guldberg, F. Bairlein, Ecological responses to recent climate change, Nature 416(6879) (2002) 389-395. https://doi.10.1038/416389a.

[10] J. Hansen, R. Ruedy, M. Sato, K. Lo, Global Surface Temperature Change, Reviews of Geophysics 48(4) (2010). https://doi.10.1029/2010rg000345.

[11] S.S. Chanisada Tuchinda, Henry W. Lim, Photoprotection by window glass, automobile glass, and sunglasses, J Am Acad Dermatol 54(5) (2006) 845-54.

https://doi.10.1016/j.jaad.2006.05.014.

[12] R.V. Fahad Almutawa, Steven Q. Wang & Henry W. Lim, Current status of photoprotection by window glass, automobile glass, window films, and sunglasses, Photodermatology, Photoimmunology & Photomedicine 29(2) (2013) 65-72. https://doi.org/10.1111/phpp.12022.

[13] J.H.L. IV, J.H.L. V, A Heattransfer textbook, 4th ed., Phlogiston Press2017.

[14] H.H. Al-Kayiem, M.F.B.M. Sidik, Y.R.A.L. Munusammy, Study on the Thermal Accumulation and Distribution Inside a parked car cabin, American Journal of Applied Sciences 7(6) (2010) 784-789.

[15] C. McLaren, J. Null, J. Quinn, Heat stress from enclosed vehicles: Moderate ambient temperatures cause significant temperature rise in enclosed vehicles, Pediatrics 116(1) (2005) E109-E112. https://doi.10.1542/peds.2004-2368.

[16] I.R. Dadour, I. Almanjahie, N.D. Fowkes, G. Keady, K. Vijayan, Temperature variations in a parked vehicle, Forensic Science International 207(1-3) (2011) 205-211. https://doi.10.1016/j.forsciint.2010.10.009.

[17] U.S.E.P. Agency, The 2019 Enviromental Protection Agency Automotive Trends Report, 2020. https://nepis.epa.gov/Exe/ZyPDF.cgi?Dockey=P100YVK3.pdf. (Accessed 10.10 2020).

[18] I.E.A.E.C. in, B.a.C.S. Programme, International Energy Agency Energy Conservation in

Buildings and Community annual report 2018,, 2019. https://www.iea-ebc.org/Data/Sites/1/media/docs/AR/ebc_annual_report_2018.pdf. (Accessed 10. 5 2020).

[19] L. Capuano, Annual Energy Outlook 2020, 2020.

https://www.eia.gov/pressroom/presentations/capuano_01292020.pdf. (Accessed 10.12 2020).

[20] S. Li, J. Peng, Y. Tan, T. Ma, X. Li, B. Hao, Study of the application potential of photovoltaic direct-driven air conditioners in different climate zones, Energy Build 226 (2020) 110387-110400. https://doi.10.1016/j.enbuild.2020.110387.

[21] W. Li, S. Fan, Nanophotonic control of thermal radiation for energy applications Invited, Opt. Express 26(12) (2018) 15995-16021. https://doi.10.1364/oe.26.015995.

[22] J. Pereira, M. Gloria Gomes, A. Moret Rodrigues, M. Almeida, Thermal, luminous and energy performance of solar control films in single-glazed windows: Use of energy performance criteria to support decision making, Energy Build. 198 (2019) 431-443. https://doi.10.1016/j.enbuild.2019.06.003.

[23] A.P. Raman, M.A. Anoma, L. Zhu, E. Rephaeli, S. Fan, Passive radiative cooling below ambient air temperature under direct sunlight, Nature 515(7528) (2014) 540-4. https://doi.10.1038/nature13883.

[24] L. Cai, A.Y. Song, W. Li, P.-C. Hsu, D. Lin, P.B. Catrysse, Y. Liu, Y. Peng, J. Chen, H. Wang, J. Xu, A. Yang, S. Fan, Y. Cui, Spectrally selective nanocomposite textile for outdoor personal cooling, Adv. Mater. 30(35) (2018) 2152-2159. https://doi.10.1002/adma.201802152.

[25] E. Rephaeli, A. Raman, S. Fan, Ultrabroadband photonic structures to achieve high-performance daytime radiative cooling, Nano Lett. 13(4) (2013) 1457-1461. https://doi.10.1021/nl4004283.

[26] J.K. Tong, X. Huang, S.V. Boriskina, J. Loomis, Y. Xu, G. Chen, Infrared-transparent visible-opaque fabrics for wearable personal thermal management, Acs Photonics 2(6) (2015) 769-778. https://doi.10.1021/acsphotonics.5b00140.

[27] S. Vall, A. Castell, Radiative cooling as low-grade energy source: A literature

review, Renewable and Sustainable Energy Reviews 77 (2017) 803-820. https://doi.10.1016/j.rser.2017.04.010.

[28] O. BW, Radiant floor cooling systems, ASHRAE J 50(9) (2008) 16–22.

[29] O. BW, Radiant floor heating in theory and practice, ASHRAE J 44(7) (2002) 19–26.

[30] K. Zhao, X.-H. Liu, Y. Jiang, Application of radiant floor cooling in large space buildings – A review, Renewable and Sustainable Energy Reviews 55 (2016) 1083-1096. https://doi.10.1016/j.rser.2015.11.028.

[31] T. Li, Y. Zhai, S. He, W. Gan, Z. Wei, M. Heidarinejad, D. Dalgo, R. Mi, X. Zhao, J. Song, J. Dai, C. Chen, A. Aili, A. Vellore, A. Martini, R. Yang, J. Srebric, X. Yi, L. Hu, A radiative cooling structural material, Science 364(6442) (2019) 760-763. https://doi.10.1126/science.aau9101.

[32] M.A. Hamdan, J. Yamin, E.M.A. Hafez, Passive cooling roof design under Jordanian climate, Sustain. Cities Soc. 5 (2012) 26-29. https://doi.10.1016/j.scs.2011.10.004.

[33] K.M. Al-Obaidi, M. Ismail, A.M. Abdul Rahman, Passive cooling techniques through reflective and radiative roofs in tropical houses in Southeast Asia: A literature review, Frontiers of Architectural Research 3(3) (2014) 283-297. https://doi.10.1016/j.foar.2014.06.002.

[34] P.-C. Hsu, C. Liu, A.Y. Song, Z. Zhang, Y. Peng, J. Xie, K. Liu, C.-L. Wu, P.B. Catrysse, L. Cai, S. Zhai, A. Majumdar, S. Fan, Y. Cui, A dual-mode textile for human body radiative heating and cooling, Sci. Adv 3 (2017) 1700895-1700903.

[35] B. Xiang, X. Yin, J. Zhang, A novel cool material: ASA (acrylonitrile-styrene-acrylate) matrix composites with solar reflective inorganic particles, Composites Science and Technology 145 (2017) 149-156.

https://doi.10.1016/j.compscitech.2017.04.007.

[36] D. Fan, H. Sun, Q. Li, Thermal control properties of radiative cooling foil based on transparent fluorinated polyimide, Sol. Energy Mater Sol. Cells 195 (2019) 250-257. https://doi.10.1016/j.solmat.2019.03.019.

[37] J.H.L.I.J.H.L. V, A Heattransfer textbook, Fourth ed., Phlogiston Press, Cambridge, Massachusetts, U.S.A., 2017.

[38] J. Yoo, H. Kim, H. Chang, W. Park, S.K. Hahn, W. Kwon, Biocompatible Organosilica Nanoparticles with Self-Encapsulated Phenyl Motifs for Effective UV Protection, ACS Appl Mater Interfaces 12(8) (2020) 9062-9069. https://doi.10.1021/acsami.9b21990.

[39] W. Xie, E. Pakdel, D. Liu, L. Sun, X. Wang, Waste-Hair-Derived Natural Melanin/TiO2 Hybrids as Highly Efficient and Stable UV-Shielding Fillers for Polyurethane Films, ACS Sustain. Chem. Eng. 8(3) (2019) 1343-1352. https://doi.10.1021/acssuschemeng.9b03514.

[40] E. Hacker, C. Horsham, D. Vagenas, L. Jones, J. Lowe, M. Janda, A Mobile Technology Intervention With Ultraviolet Radiation Dosimeters and Smartphone Apps for Skin Cancer Prevention in Young Adults: Randomized Controlled Trial, JMIR Mhealth Uhealth 6(11) (2018) 1-13. https://doi.10.2196/mhealth.9854.

[41] Q. Liu, J. Toudert, F. Liu, P. Mantilla-Perez, M.M. Bajo, T.P. Russell, J. Martorell, Circumventing UV Light Induced Nanomorphology Disorder to Achieve Long Lifetime PTB7-Th:PCBM Based Solar Cells, Adv Energy Mater 7(21) (2017) 1701201-1701228. https://doi.10.1002/aenm.201701201.

[42] Y. Feng, J. Zhang, J. He, J. Zhang, Transparent cellulose/polyhedral oligomeric silsesquioxane nanocomposites with enhanced UV-shielding properties, Carbohydr Polym 147 (2016) 171-177. https://doi.10.1016/j.carbpol.2016.04.003.

[43] J. Li, X. Zhang, J. Zhang, Q. Mi, F. Jia, J. Wu, J. Yu, J. Zhang, Direct and complete utilization of agricultural straw to fabricate all-biomass films with high-strength, high-haze and UV-shielding properties, Carbohydr Polym 223 (2019) 115057-115064. https://doi.10.1016/j.carbpol.2019.115057.

[44] C. Han, F. Wang, C. Gao, P. Liu, Y. Ding, S. Zhang, M. Yang, Transparent epoxy–ZnO/CdS nanocomposites with tunable UV and blue light-shielding capabilities, J. Mater. Chem. C 3(19) (2015) 5065-5072. https://doi.10.1039/c4tc02880e.

[45] W. Wang, B. Zhang, S. Jiang, H. Bai, S. Zhang, Use of CeO(2) Nanoparticles to Enhance UV-Shielding of Transparent Regenerated Cellulose Films, Polymers 11(3) (2019) 458-471. https://doi.10.3390/polym11030458.

[46] S. Gamage, E.S.H. Kang, C. Åkerlind, S. Sardar, J. Edberg, H. Kariis, T. Ederth, M. Berggren, M.P. Jonsson, Transparent nanocellulose metamaterial enables controlled optical diffusion and radiative cooling, J. Mater. Chem. C 8(34) (2020) 11687-11694. https://doi.10.1039/d0tc01226b.

[47] E. Manias, A. Touny, L. Wu, K. Strawhecker, B. Lu, T.C. Chung, Polypropylene/Montmorillonite Nanocomposites. Review of the Synthetic Routes and Materials Properties, Chem. Mater 13(10) (2001) 3516-3523. https://doi.10.1021/cm0110627.

[48] T. Hanemann, D.V. Szabó, Polymer-Nanoparticle Composites: From Synthesis to Modern Applications, Materials 3(6) (2010) 3468-3517. https://doi.10.3390/ma3063468.

[49] C.-c. Jiang, Y.-k. Cao, G.-y. Xiao, R.-f. Zhu, Y.-p. Lu, A review on the application of inorganic nanoparticles in chemical surface coatings on metallic substrates, RSC Adv 7(13) (2017) 7531-7539. https://doi.10.1039/c6ra25841g.

[50] D.J. Kim, M.J. Jo, S.Y. Nam, A review of polymer–nanocomposite electrolyte membranes for fuel cell application, Ind. Eng. Chem. Res. 21 (2015) 36-52.

https://doi.10.1016/j.jiec.2014.04.030.

[51] Y. Liang, W.H. Lai, Z. Miao, S.L. Chou, Nanocomposite Materials for the Sodium-Ion Battery: A Review, Small 14(5) (2018). https://doi.10.1002/smll.201702514.

[52] S. Kango, S. Kalia, A. Celli, J. Njuguna, Y. Habibi, R. Kumar, Surface modification of inorganic nanoparticles for development of organic–inorganic nanocomposites—A review, Progress in Polymer Science 38(8) (2013) 1232-1261. https://doi.10.1016/j.progpolymsci.2013.02.003.

[53] M.Z. Rong, M.Q. Zhang, W.H. Ruan, Surface modification of nanoscale fillers for improving properties of polymer nanocomposites: a review, Materials Science and Technology 22(7) (2013) 787-796. https://doi.10.1179/174328406x101247.

[54] M.E. El-Naggar, A.G. Hassabo, A.L. Mohamed, T.I. Shaheen, Surface modification of SiO2 coated ZnO nanoparticles for multifunctional cotton fabrics, J Colloid Interface Sci 498 (2017) 413-422. https://doi.10.1016/j.jcis.2017.03.080.

[55] R. Hong, T. Pan, J. Qian, H. Li, Synthesis and surface modification of ZnO nanoparticles, Chem. Eng. J. 119(2-3) (2006) 71-81. https://doi.10.1016/j.cej.2006.03.003.

[56] M. Kathalewar, A. Sabnis, G. Waghoo, Effect of incorporation of surface treated zinc oxide on non-isocyanate polyurethane based nano-composite coatings, Progress in Organic Coatings 76(9) (2013) 1215-1229. https://doi.10.1016/j.porgcoat.2013.03.027.

[57] H. Hashimoto, R. Tanino, M. Nakamura, Y. Fujita, Surface Treatment of Zinc Oxide Nanoparticles by Silica Coating and Evaluation of Their Dispersibility and Photoluminescent Properties, e-Journal of Surface Science and Nanotechnology 13(0) (2015) 451-454. https://doi.10.1380/ejssnt.2015.451.

[58] A. Pud, N. Ogurtsov, A. Korzhenko, G. Shapoval, Some aspects of preparation methods and properties of polyaniline blends and composites with organic polymers,

Prog. poly. sci. 28(12) (2003) 1701-1753. https://doi.10.1016/j.progpolymsci.2003.08.001.

[59] S.S. Ray, M. Okamoto, Polymer/layered silicate nanocomposites: a review from preparation to processing, Progress in polymer science 28(11) (2003) 1539-1641. https://doi.10.1016/j.progpolymsci.2003.08.002.

[60] M. Amin, Methods for preparation of nano-composites for outdoor insulation applications, Rev. Adv. Mater. Sci 34 (2013) 173-184.

[61] B. Bharath Kumar, S.E. Zeltmann, M. Doddamani, N. Gupta, S. Gurupadu, R. Sailaja, Effect of cenosphere surface treatment and blending method on the tensile properties of thermoplastic matrix syntactic foams, J. Appl. Polym. Sci. 133(35) (2016) 1-11. https://doi.10.1002/app.43881.

[62] L. Cai, A.Y. Song, W. Li, P.C. Hsu, D. Lin, P.B. Catrysse, Y. Liu, Y. Peng, J. Chen, H. Wang, J. Xu, A. Yang, S. Fan, Y. Cui, Spectrally Selective Nanocomposite Textile for Outdoor Personal Cooling, Adv Mater 30(35) (2018) e1802152. https://doi.10.1002/adma.201802152.

[63] A. Emamifar, M. Mohammadizadeh, Preparation and application of LDPE/ZnO nanocomposites for extending shelf life of fresh strawberries, Food technology and biotechnology 53(4) (2015) 488-495. https://doi.10.17113/ftb.53.04.15.3817.

[64] P.A. Zapata, L. Tamayo, M. Paez, E. Cerda, I. Azocar, F.M. Rabagliati, Nanocomposites based on polyethylene and nanosilver particles produced by metallocenic "in situ" polymerization: synthesis, characterization, and antimicrobial behavior, Eur. Polym. J. 47(8) (2011) 1541-1549. https://doi.10.1016/j.eurpolymj.2011.05.008.

[65] Z. Xu, C. Gao, In situPolymerization Approach to Graphene-Reinforced Nylon-6 Composites, Macromolecules 43(16) (2010) 6716-6723.

https://doi.10.1021/ma1009337.

[66] E. Tang, G. Cheng, X. Ma, Preparation of nano-ZnO/PMMA composite particles via grafting of the copolymer onto the surface of zinc oxide nanoparticles, Powder Technol. 161(3) (2006) 209-214. https://doi.10.1016/j.powtec.2005.10.007.

[67] M. Zarrinkhameh, A. Zendehnam, S.M. Hosseini, Fabrication of polyvinylchloride based nanocomposite thin film filled with zinc oxide nanoparticles: Morphological, thermal and optical characteristics, J Ind Eng Chem 30 (2015) 295-301. https://doi.10.1016/j.jiec.2015.05.036.

[68] M.E. Mackay, A. Tuteja, P.M. Duxbury, C.J. Hawker, B. Van Horn, Z.B. Guan, G.H. Chen, R.S. Krishnan, General strategies for nanoparticle dispersion, Science 311(5768) (2006) 1740-1743. https://doi.10.1126/science.1122225.

[69] B.A. Miller-Chou, J.L. Koenig, A review of polymer dissolution, Progress in Polymer Science 28(8) (2003) 1223-1270. https://doi.10.1016/s0079-6700(03)00045-5.

[70] M.M. Sebastian Koltzenburg, Oskar Nuyken, Polymer Chemistry, Springer, New York, 2017.

[71] W. Bond, Measurement of the refractive indices of several crystals, J Appl Phys 36(5) (1965) 1674-1677. https://doi..org/10.1063/1.1703106.

[72] J.V. Gulmine, P.R. Janissek, H.M. Heise, L. Akcelrud, Polyethylene characterization by FTIR, Polym Test 21(5) (2002) 557-563. https://doi.10.1016/s0142-9418(01)00124-6.

[73] A.T. Young, Rayleigh scattering, Appl. Opt. 20(4) (1981) 533-535. https://doi.10.1364/ao.20.000533.

[74] P.C. Hiemenz, T.P. Lodge, Polymer chemistry, CRC press2007.

Chapter 2　Preparation of flexible transparent spectrum selective films

Chapter 2 Preparation of flexible transparent spectrum selective films

2.1 Introduction

NPs are popularly utilized for the property promotion and functionalization of polymeric materials for advantageous electrical, optical, or mechanical properties [1-3] in more than past two decades. ZnO NPs has been used in developing functional devices, catalysts, pigments, optical materials, cosmetics, and UV absorbers [4-6]. The biggest challenge is how to uniformly disperse NPs in polymers for better functional performances [7]. If there is serious NP agglomeration in composites, the functions of inorganic-organic composites would be hindered as Li and coworkers reported [8]. UV photon is high-energy thermal waves [9], which reach the earth's surface more than before because of the increased ozone depletion as indicated by Yoo et al. [10] and Xie et al. [11]. The UV photons can not only cause serious injuries to the skin which might eventually result in skin cancer as Hacker et al. reported [12], but also provide radiative heat which may consume much energy to regulate temperature in space [13]. More and more attention has been paid for shielding UV photons in recent years. Feng et al. [14] and Li et al. [15] fabricated transparent UV-shielding composites using cellulose, though the material is hard for large scale production.

Han et al. [16] used 60 nm NPs mixed into a polymer, and finally the NPs were agglomerated into 600 nm clusters. Complete UV-shielding performance would appear when the NP concentration reached above 7%, which would influence the transparency to visible light. Wang et al. [17] fabricated similar functional materials by mixing inorganic NPs with polymers, which also had a high NP concentration about 0.5 mol/ml. UV-shielding materials also can be a good candidate for passive cooling, which have the cooling function without any kinds of energy input. Li et al. fabricated opaque textile for outdoor personal cooling by shielding UV and high energy visible lights [18]. Gamage et al. have shown that UV-shielding and visible transparent materials are good candidates for passive cooling to save energy consumption [19].

The most common methods reported fabricating UV-shielding materials are combining polymer and inorganic semiconductor NPs. In order to improve the compatibility between NPs and polymers, surface treatments have been applied to modify the surface properties of NPs [20]. However, these treatments have the potential to induce adverse effects on the catalytic, optical, or magnetic properties of the surface-treated NPs. This may greatly influence the intended performance of the composites. Jiang et al. reported that the coating processes of NP may be phased out because of their possible high-cost or harmful effects [21]. El-Naggar and coworkers employed the core/shell structure to improve the agglomeration of ZnO NPs; however, the characteristic absorption peaks of the NPs were shielded [22]. In addition, Hong et al. reported reduced catalytic activity of coated ZnO NPs [23]. Therefore, direct doping of pristine NPs into the polymer could be preferable if one could achieve uniform dispersion of the NPs in the polymer when optimal mixing

strategies could be adopted. Mackay et al. reported that thermodynamically stable dispersion of nanoparticles into a polymeric liquid enhanced the dispersion of nanoparticles by increasing the enthalpy gain of the solution system [24].

Solution methods are relatively easy to achieve an even dispersion of NPs in polymers, especially those without a melting temperature or with a high molten viscosity as reported by Zarrinkhameh et al. [25]. In recent decades, various approaches have been attempted for the dispersion of NPs in polymers, including solution dispersion, mechanical blending and in situ polymerization with NPs reported by Guo et al. [26], each method has their own advantages and disadvantages reported by Ray et al. [27]. Polyolefins are synthesized via addition polymerization and thus have a relatively high degree of polymerization, which results in high molten viscosity [28]. Moreover, they are hard to dissolve in a solution without high temperature and long durations due to the saturated chemical structures, thus leading to poor affiliation with most of the organic solvents. Therefore, polyolefin solutions are often highly dilute in the published literatures. Blackadder and Schleinitz dissolved low-density polyethylene (LDPE) in n-dodecane, p-xylene, and decalin solvents at 0.1 wt%, 0.375 wt%, 0.75 wt%, 1.00 wt%, and 1.5 wt% to obtain single crystals [29]. Kong et al. reported the use of 0.7 wt% of polyethylene (PE) solution to determine the routes of solution fractionation [30]. Wong and coauthors dissolved LDPE at 1.1 wt%–6.5 wt% to convert plastic waste from solid to liquid to transport it via feeding pipelines [31].

However, in the published literatures, reports on the range of PE concentrations and experimental conditions in which virgin inorganic NPs can be well dispersed are scarce.

NP diffusion in a polymer solution is largely dependent on the viscosity of the solution which is also dependent on the polymer concentration and temperature, in addition to the dissolution time of the polymer solution. Thus, a systematic study was conducted to determine the optimal casting temperature, LDPE concentration, and dissolution time for uniform dispersion of inorganic NPs in LDPE using the solution-casting method. This ZnO NP/LDPE composite film exhibits spectrum selective properties for shielding UV and diminishing transmittance of visible light and thus could be potentially used as a passive cooling material for the purpose of energy conservation. Therefore, the transmissivities of the films with different NP concentrations were also evaluated.

2.2 Preparation and characterization on of samples

LDPE pellets (AS: 9002-88-4) with a melting index of 25 g/10 min were purchased from Alorich Chemistry. ZnO NPs with an average diameter of 90 nm were provided by Rhawn Company in Shanghai, China. In the sample preparation, first, the ZnO NPs were dissolved in 12 g of xylene [32] (Achilias *et al*.) by sonication for 12 min at a frequency of 22 kHz in an ultrasonic cell disruptor (Scientz-IID) with a 6-mm-diameter probe in a glass column at an ambient temperature. Then, the LDPE pellets were added into the solution in the glass column using a magnetic stirrer and heated in oil bath. Once the solution was homogenized after stirring for sufficient time at a high temperature, it was casted to form a primary film. Finally, the thickness of the casted film was adjusted by hot pressing and cooling down. The conditions for film fabrication are presented in **Table 2-1**. There designed 3 groups

experiments marked as a, b, c in Table 2-1.

Table 2-1. Conditions for film formation experiments

Group	Temperature of casting (ºC)	Concentration of LDPE: xylene (%)	Duration of dissolution (h)	Temperature of oil bath (ºC)	Concentration of ZnO: LEPD (%)
1	5 50 75 105 115 115 (in vacuum) a	5	96	105	4%
2	115 (in vacuum)	2.4 3.8 6.1 7.0 8.1 9 b	156	105	4%
3	115 (in vacuum)	3.2%	90 120 188 202 322 c	105	4%

From the above experiments, we were able to select a set of optimal conditions, i.e., 3.2% LDPE-xylene solution, 105 °C dissolution temperature and 322-h dissolution time, and 115 °C in vacuum oven for the formation of casted films with reasonably good particle dispersion. Using these conditions, we selected three group conditions marked as a, b, c (**Table 2-2**.) to optimize the transmissivity of the flexible films with balanced performance of UV-shielding and transparency for visible light. In which the NP concentrations, (namely, 4%, 5%, 6% ZnO NPs), different NP size, (20 nm, 50 nm and 90 nm), and different hot post procedures, (quenched samples or cooling samples by ambient temperature), were selected to carried out. And also the flexural strength would be influenced by the NP concentration, NP size and hot post procedures which reported by Wu et al. [33].

Table 2-2. Optimizing the experimental parameters of membrane formation experiments

Group	Concentration of ZnO:LEPD (%)	Diameter of NP (nm)	Thickness (μm)	Post processes of hot press
1	4	20 a 50 90	120±5	Ambient cooled
2	4 b 5 6	90	120±5	Ambient cooled
3	6	90	120±5	Quenched or ambient cooled c

2.3 Characterization of samples

2.3.1 Microscopy test

The surfaces of the films, corresponding elemental mapping, and analysis were examined with a field-emission scanning electron microscope (FE-SEM: Zeiss MERLIN, Oberkochen, Germany). The samples were sprayed with Au for 45s before imaging.

2.3.2 X-ray diffraction analysis

X-ray diffraction (XRD) was performed on the films using a MiniFlex 300 (Rigaku Corporation, Japan). The scan range was set between 10° and 80° and the scan rate was 0.04 °/s. The tube voltage and experimental current were 40 kV and 20 mA, respectively.

2.3.3 Transmittance test

The transmittance tests for the spectrum selective films were conducted using an ultraviolet–visible–near-infrared (UV–Vis–NIR) spectrophotometer (Yokogawa Model AQ6375B).

2.3.4 Mechanical and thermal test

Films were tensile tested at 25 °C and 60% relative humidity using a universal testing

machine (Model Instron Microtester 5948) at a gage length of 10 mm and specimen width of 2 mm at a strain rate of 0.10/min with a load cell of 100 N capacity.

The thermal properties of the films were determined using a deferential scanning calorimeter (DSC) (Model CCTA DSC25) in nitrogen. Thermal properties of the films were determined using deferential scanning calorimetry (DSC) in nitrogen on a machine Model CCTA DSC25. The specimens were equilibrated at -80 °C for 2 min and then heated at 10 °C/min to 300 °C at which they were isothermal for 2 min, and then cooled down at 10 °C/min to -80.00 °C.

References

[1] T.E. Anna C. Balazs, Thomas P. Russell, Nanoparticle Polymer Composites: Where Two Small Worlds Meet, Sci 314 (2006) 1107-1110. https://doi. 10.1126/science.1130557.

[2] D.J. Kim, M.J. Jo, S.Y. Nam, A review of polymer–nanocomposite electrolyte membranes for fuel cell application, Ind. Eng. Chem. Res. 21 (2015) 36-52. https://doi.10.1016/j.jiec.2014.04.030.

[3] R. Xiong, K. Hu, A.M. Grant, R. Ma, W. Xu, C. Lu, X. Zhang, V.V. Tsukruk, Ultrarobust Transparent Cellulose Nanocrystal-Graphene Membranes with High Electrical Conductivity, Adv. Mater. 28(7) (2016) 1501-9. https://doi.10.1002/adma.201504438.

[4] K. Oksman, Y. Aitomäki, A.P. Mathew, G. Siqueira, Q. Zhou, S. Butylina, S. Tanpichai, X. Zhou, S. Hooshmand, Review of the recent developments in cellulose nanocomposite

processing, Compos. Part A Appl. Sci. Manuf. 83 (2016) 2-18. https://doi.10.1016/j.compositesa.2015.10.041.

[5] K.-T. Lau, D. Hui, The revolutionary creation of new advanced materials--carbon nanotube composites, Compos. B. Eng. 33 (2002) 263-277.

[6] K. Li, S. Jin, J. Li, H. Chen, Improvement in antibacterial and functional properties of mussel-inspired cellulose nanofibrils/gelatin nanocomposites incorporated with graphene oxide for active packaging, Ind Crops Prod 132 (2019) 197-212. https://doi.10.1016/j.indcrop.2019.02.011.

[7] F. Li, H.-Y. Yu, Y.-Y. Wang, Y. Zhou, H. Zhang, J.-M. Yao, S.Y.H. Abdalkarim, K.C. Tam, Natural Biodegradable Poly(3-hydroxybutyrate-co-3-hydroxyvalerate) Nanocomposites with Multifunctional Cellulose Nanocrystals/Graphene Oxide Hybrids for High-Performance Food Packaging, J. Agric. Food. Chem. 67(39) (2019) 10954-10967. https://doi.10.1021/acs.jafc.9b03110.

[8] J.H.L.I.J.H.L. V, A Heattransfer textbook, Fourth ed., Phlogiston Press, Cambridge, Massachusetts, U.S.A., 2017.

[9] J. Yoo, H. Kim, H. Chang, W. Park, S.K. Hahn, W. Kwon, Biocompatible Organosilica Nanoparticles with Self-Encapsulated Phenyl Motifs for Effective UV Protection, ACS Appl Mater Interfaces 12(8) (2020) 9062-9069. https://doi.10.1021/acsami.9b21990.

[10] W. Xie, E. Pakdel, D. Liu, L. Sun, X. Wang, Waste-Hair-Derived Natural Melanin/TiO2 Hybrids as Highly Efficient and Stable UV-Shielding Fillers for Polyurethane Films, ACS Sustain. Chem. Eng. 8(3) (2019) 1343-1352. https://doi.10.1021/acssuschemeng.9b03514.

[11] E. Hacker, C. Horsham, D. Vagenas, L. Jones, J. Lowe, M. Janda, A Mobile Technology Intervention With Ultraviolet Radiation Dosimeters and Smartphone Apps for Skin Cancer Prevention in Young Adults: Randomized Controlled Trial, JMIR Mhealth Uhealth 6(11) (2018) 1-13. https://doi.10.2196/mhealth.9854.

[12] S. Li, J. Peng, Y. Tan, T. Ma, X. Li, B. Hao, Study of the application potential of photovoltaic direct-driven air conditioners in different climate zones, Energy Build 226 (2020) 110387-110400. https://doi.10.1016/j.enbuild.2020.110387.

[13] Q. Liu, J. Toudert, F. Liu, P. Mantilla-Perez, M.M. Bajo, T.P. Russell, J. Martorell, Circumventing UV Light Induced Nanomorphology Disorder to Achieve Long Lifetime PTB7-Th:PCBM Based Solar Cells, Adv Energy Mater 7(21) (2017) 1701201-1701228. https://doi.10.1002/aenm.201701201.

[14] Y. Feng, J. Zhang, J. He, J. Zhang, Transparent cellulose/polyhedral oligomeric silsesquioxane nanocomposites with enhanced UV-shielding properties, Carbohydr. Polym. 147 (2016) 171-177. https://doi.10.1016/j.carbpol.2016.04.003.

[15] J. Li, X. Zhang, J. Zhang, Q. Mi, F. Jia, J. Wu, J. Yu, J. Zhang, Direct and complete utilization of agricultural straw to fabricate all-biomass films with high-strength, high-haze and UV-shielding properties, Carbohydr. Polym. 223 (2019) 115057-115064. https://doi.10.1016/j.carbpol.2019.115057.

[16] C. Han, F. Wang, C. Gao, P. Liu, Y. Ding, S. Zhang, M. Yang, Transparent epoxy–ZnO/CdS nanocomposites with tunable UV and blue light-shielding capabilities, J. Mater. Chem. C 3(19) (2015) 5065-5072. https://doi.10.1039/c4tc02880e.

[17] W. Wang, B. Zhang, S. Jiang, H. Bai, S. Zhang, Use of CeO(2) Nanoparticles to

Enhance UV-Shielding of Transparent Regenerated Cellulose Films, Polymers 11(3) (2019) 458-471. https://doi.10.3390/polym11030458.

[18] T. Li, Y. Zhai, S. He, W. Gan, Z. Wei, M. Heidarinejad, D. Dalgo, R. Mi, X. Zhao, J. Song, J. Dai, C. Chen, A. Aili, A. Vellore, A. Martini, R. Yang, J. Srebric, X. Yi, L. Hu, A radiative cooling structural material, Sci 364(6442) (2019) 763- 760. https://doi.10.1126/science.aau9101.

[19] S. Gamage, E.S.H. Kang, C. Åkerlind, S. Sardar, J. Edberg, H. Kariis, T. Ederth, M. Berggren, M.P. Jonsson, Transparent nanocellulose metamaterial enables controlled optical diffusion and radiative cooling, J. Mater. Chem. C 8(34) (2020) 11687-11694. https://doi.10.1039/d0tc01226b.

[20] S. Kango, S. Kalia, A. Celli, J. Njuguna, Y. Habibi, R. Kumar, Surface modification of inorganic nanoparticles for development of organic–inorganic nanocomposites—A review, Prog. Polym. Sci. 38(8) (2013) 1232-1261. https://doi.10.1016/j.progpolymsci.2013.02.003.

[21] C.-c. Jiang, Y.-k. Cao, G.-y. Xiao, R.-f. Zhu, Y.-p. Lu, A review on the application of inorganic nanoparticles in chemical surface coatings on metallic substrates, RSC Adv 7(13) (2017) 7531-7539. https://doi.10.1039/c6ra25841g.

[22] M.E. El-Naggar, A.G. Hassabo, A.L. Mohamed, T.I. Shaheen, Surface modification of SiO2 coated ZnO nanoparticles for multifunctional cotton fabrics, J. Colloid Interface Sci. 498 (2017) 413-422. https://doi.10.1016/j.jcis.2017.03.080.

[23] R. Hong, T. Pan, J. Qian, H. Li, Synthesis and surface modification of ZnO nanoparticles, Chem. Eng. J. 119(2-3) (2006) 71-81. https://doi.10.1016/j.cej.2006.03.003.

[24] U. Moonart, S. Utara, Effect of surface treatments and filler loading on the properties of hemp fiber/natural rubber composites, Cellu 26(12) (2019) 7271-7295. https://doi.10.1007/s10570-019-02611-w.

[25] A.T. Michael E. Mackay, Phillip M. Duxbury, Craig J. Hawker3, Brooke Van Horn, Zhibin Guan, Guanghui, General strategies for nanoparticle dispersion, Sci 311(5768) (2006) 1740-1743.

[26] M. Zarrinkhameh, A. Zendehnam, S.M. Hosseini, Fabrication of polyvinylchloride based nanocomposite thin film filled with zinc oxide nanoparticles: Morphological, thermal and optical characteristics, J Ind Eng Chem 30 (2015) 295-301. https://doi.10.1016/j.jiec.2015.05.036.

[27] S. Guo, D. Fu, A. Utupova, D. Sun, M. Zhou, Z. Jin, K. Zhao, Applications of polymer-based nanoparticles in vaccine field, Nanotechnol. Rev. 8(1) (2019) 143-155. https://doi.10.1515/ntrev-2019-0014.

[28] S.S. Ray, M. Okamoto, Polymer/layered silicate nanocomposites: a review from preparation to processing, Prog. Polym. Sci. 28(11) (2003) 1539-1641. https://doi.10.1016/j.progpolymsci.2003.08.002.

[29] P.C. Hiemenz, T.P. Lodge, Polymer chemistry, CRC press2007.

[30] D. Blackadder, H. Schleinitz, The dissolution and recrystallization of polyethylene crystals suspended in various solvents, Poly 7(12) (1966) 603-637.

[31] J. Kong, X. Fan, M. Jia, Study of polyethylene solution fractionation and resulting fractional crystallization behavior, J. Appl. Polym. Sci. 93(6) (2004) 2542-2549.

[32] S.L. Wong, N. Ngadi, T.A.T. Abdullah, Study on Dissolution of Low Density

Polyethylene (LDPE), Appl. Mech. Mater. 695 (2014) 170-173. https://doi.10.4028/www.scientific.net/AMM.695.170.

[33] M.M. Sebastian Koltzenburg, Oskar Nuyken, Polymer Chemistry, Springer, New York, 2017.

[34] S.L. Shenoy, W.D. Bates, H.L. Frisch, G.E. Wnek, Role of chain entanglements on fiber formation during electrospinning of polymer solutions: good solvent, non-specific polymer–polymer interaction limit, Poly 46(10) (2005) 3372-3384. https://doi.10.1016/j.polymer.2005.03.011.

[35] J. Choi, M.J.A. Hore, N. Clarke, K.I. Winey, R.J. Composto, Nanoparticle Brush Architecture Controls Polymer Diffusion in Nanocomposites, Macromolecules 47(7) (2014) 2404-2410. https://doi.10.1021/ma500235v.

[36] M. Belmares, M. Blanco, W.A. Goddard, 3rd, R.B. Ross, G. Caldwell, S.H. Chou, J. Pham, P.M. Olofson, C. Thomas, Hildebrand and Hansen solubility parameters from molecular dynamics with applications to electronic nose polymer sensors, J. Comput. Chem. 25(15) (2004) 1814-26. https://doi.10.1002/jcc.20098.

[37] D.S. Achilias, C. Roupakias, P. Megalokonomos, A.A. Lappas, E.V. Antonakou, Chemical recycling of plastic wastes made from polyethylene (LDPE and HDPE) and polypropylene (PP), J. Hazard. Mater. 149(3) (2007) 536-42. https://doi.10.1016/j.jhazmat.2007.06.076.

[38] Y. Wu, B. Tang, K. Liu, X. Zeng, J. Lu, T. Zhang, X. Shen, Enhanced flexural properties of aramid fiber/epoxy composites by graphene oxide, Nanotechnol. Rev. 8(1) (2019) 484-492. https://doi.10.1515/ntrev-2019-0043.

Chapter 3　Properties of transparent spectrum selective ZnO/LDPE film

Chapter 3 Properties of transparent spectrum selective ZnO/LDPE films

3.1 Conditions of fabricating ZnO/LDPE nanocomposites

3.1.1 Principles for Material Selection

LDPE is a semi-crystalline polymer with long molecular chains [1]. Selecting proper solute is critical for the dissolution of LDPE. According to the Gibbs-Helmholtz equation [2]:

$$\Delta G_m = \Delta H_m - T * \Delta S_m \quad (3\text{-}1)$$

where ΔG_m, ΔH_m, and ΔS_m denote the changes in Gibbs free energy, enthalpy, and entropy on mixing, respectively, and T denotes the absolute temperature. A negative ΔG_m indicates that the mixing process occurs spontaneously. In a good solvent, Shenoy et al. reported the interactions between the polymer and solvent are favorable to the interactions between individual polymer segments [3]. This results in the expansion of polymer coils. If the distance between the neighboring polymer chains is larger than the diameter of the NPs, both the solvent molecules and NPs can penetrate the polymer according Choi et al.

reported [4]. Contrarily, in a poor solvent, the coil collapses. In the transition from a good solvent to a poor solvent, a so-called θ-solution is formed, and the corresponding temperature is called θ-temperature, at which $\Delta G_m = 0$ [2]. In other words, at θ-temperature, the interaction between the polymer segments is equally favorable to that between the solvent and polymer segments. This indicates that the polymer chains are in a stable state, thus allowing the NPs to travel freely if the distances between either neighboring polymer segments are larger than the NPs size[5].

For semi-crystalline polymers, dissolution is an endothermic process [2]. In addition, the enthalpy of the LDPE solution can be calculated using the Hildebrand solubility principle equation [6]:

$$\Delta H_m = V_m \varphi_1 \varphi_2 [\delta_1 - \delta_2]^2 \qquad (3\text{-}2)$$

where V_m denotes the volume of mixture or solution; φ_1 and φ_2, the volume fractions of solvent and solute, respectively; and δ_1 and δ_2, the solubility parameters of the solvent and solute, respectively. According to the Hildebrand solubility principle, the enthalpy of the solution could be minimized if the solubility parameters of the solvent and solute are close to each other. This could make the dissolution relatively easy. Since the solubility parameter of LDPE is 7.9-8.1 $(cal^{0.5}cm^{-3})^{1/2}$ [2] and that of xylene is 8.75 $(cal^{0.5}cm^{-3})^{1/2}$ [2], xylene was chosen as the solvent to dissolve LDPE.

Table 2-3. The enthalpy of the different concentrations of the LDPE solvent

Items	Solution (LDPE in xylene)					
LDPE (wt%)	2	4	6	8	10	12
ΔH_m (cal)	0.78	1.47	2.27	3.01	3.75	4.50

For the different concentrations of the LDPE solution in 12 g of xylene, the enthalpies are all positive, as presented in Table 2, which were calculated using Equation 3-2. According to the Gibbs–Helmholtz equation, the bigger the enthalpy of the solution, the more difficult the dissolution of the polymer in xylene. That means that a higher temperature or additional entropy should be provided to the solution system, which would make the changes in Gibbs free energy close to zero or a negative value [2]. Therefore, the solution needs to be heated to a temperature close to the melting point of the polymer to dissolve its crystalline region. The boiling point of xylene is 144.3 °C [7], and the dissolution was performed in an oil bath at 105 °C ± 3 °C. Moreover, the solution should be kept at the temperature, namely 105 °C, for a long time with a magnetic stirrer at the bottom of the beaker to provide additional entropy to the solution system according to Mackay and coworker's points [5].

3.1.2 Effect of casting temperature

Fig. 3-1 presents the films formed at different casting or volatilization temperatures ranging from 5 ℃ to 115 ℃. At 5 ℃, the casted film looked like fine powder, and at 50 ℃, it appeared as a white opaque pancake-like film with cracks on the surface. At 75 ℃, the film looked like a combination of white powder, white pancake, and semitransparent film. At 105 ℃, a white opaque uniform film was formed. The films presented in Figure 1e and 1f were formed in vacuum oven and ordinary oven, respectively, at 115 ℃. Both were relatively transparent and uniform, although the film formed in air in a regular oven appeared slightly yellowish possibly due to oxidation.

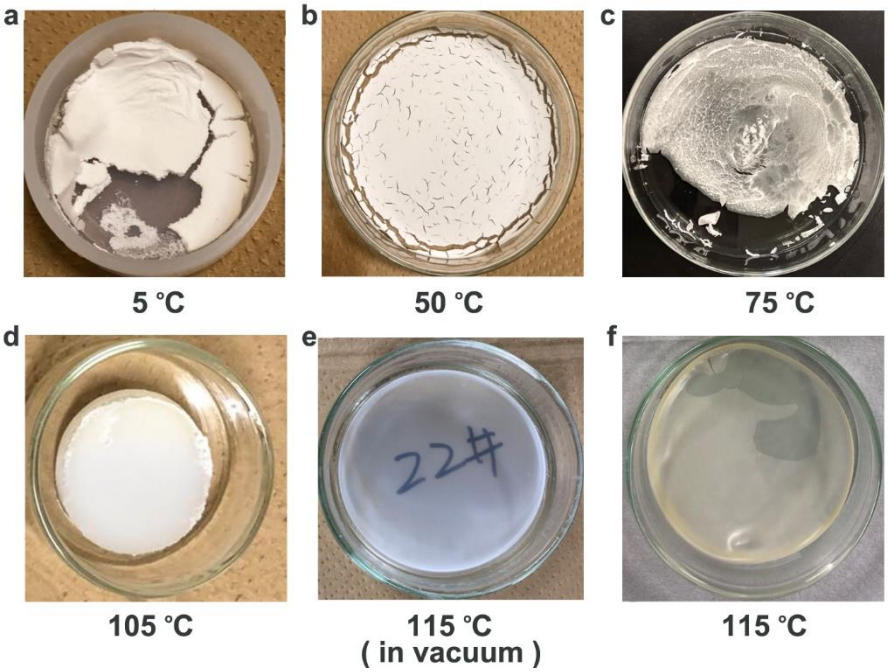

Fig. 3-1. Casted ZnO NP (4wt%)/LDPE films formed at different casting temperatures.

The morphologies of the films formed at different temperatures revealed the states of the molecules in the solution during the volatilization of the solvent. As discussed in the

previous section, mixing the polymer with the solvent is a spontaneous process when $\Delta G_m < 0$. This could only occur when the temperature was sufficiently high, according to Equation 2-1 [2]. When the solution temperature was low, the polymer molecules tended to exhibit phase separation with the solvent and thus formed clusters of polymer molecules in the solution, which then became polymer particles after the evaporation of the solvent. As the temperature increased, the molecules had higher affiliation with the solvent and thus were less and less likely to exhibit phase separation in the solution. Even if some degree of phase separation still existed, the molecules on the boundaries between the neighboring domains of polymers were likely entangled. Thus, the polymer particles formed at higher temperatures, for example, 50 °C to 75 °C, were stuck together, forming a powdery cake. These films could develop cracks due to the differential shrinkage of the different parts of the film caused by the uneven distribution of the polymer phases. As the casting temperature increased, exceeding the θ temperature, the polymer molecules in the solution exhibited good solubility and thus did not demonstrate phase separation during the evaporation of the solvent [2]. This made the casted film transparent and free of cracks.

3.1.3 The solubility of LDPE in different concentrations

To determine the proper concentration for the dissolution of LDPE with reasonably good dispersion of the NPs, a systematic experiment was conducted at LDPE concentrations of 2.4 wt%, 3.8 wt%, 6.1 wt%, 7.0 wt%, 8.1 wt%, and 9.0 wt%. Such concentrations are close to those presented in Table 1. The surface morphology and particle cluster sizes of the films are presented in **Fig. 3-2**. The film surfaces became rougher as the LDPE concentration increased. More importantly, the peak size of the NP cluster also increased from 0.8 to 2.3 μm as the LDPE concentration increased from 6.1% to 9.0%. Below 6.1%, the peak cluster size of 0.8 μm was maintained, regardless of the concentration reduction, which has the similar report on Ali et al research [8]. Obviously, when the LDPE concentration increases, the enthalpy ΔH_m of the polymer solution will be increased as shown in Table 2 (ΔH_m increases almost 5 times for polymer concentration increasing from 2 to 10 wt%), which means a higher temperature and longer time will be required for the same degree of solubility of LDPE in the solution according to Equation 2-1. This would hinder the dissolution of the polymer, increase the solution viscosity, and inhibit the dispersion of the NPs [9]. It is noteworthy that the films were prepared with a dissolution time of 156 h at 105 °C, which may not be sufficiently long for the complete dispersion of individual NPs, as discussed in the subsequent section. In our later experiments, we greatly prolonged the dissolution time and were able to achieve satisfactory dispersion of NPs with peak diameter similar to that of the individual NPs. Evidently, this result implies that a concentration below 6% is preferred for a good initial dispersion of the NPs. In the following experiment, we selected 3.2% of LDPE and prolonged the dissolution time for further dispersion of the

NPs.

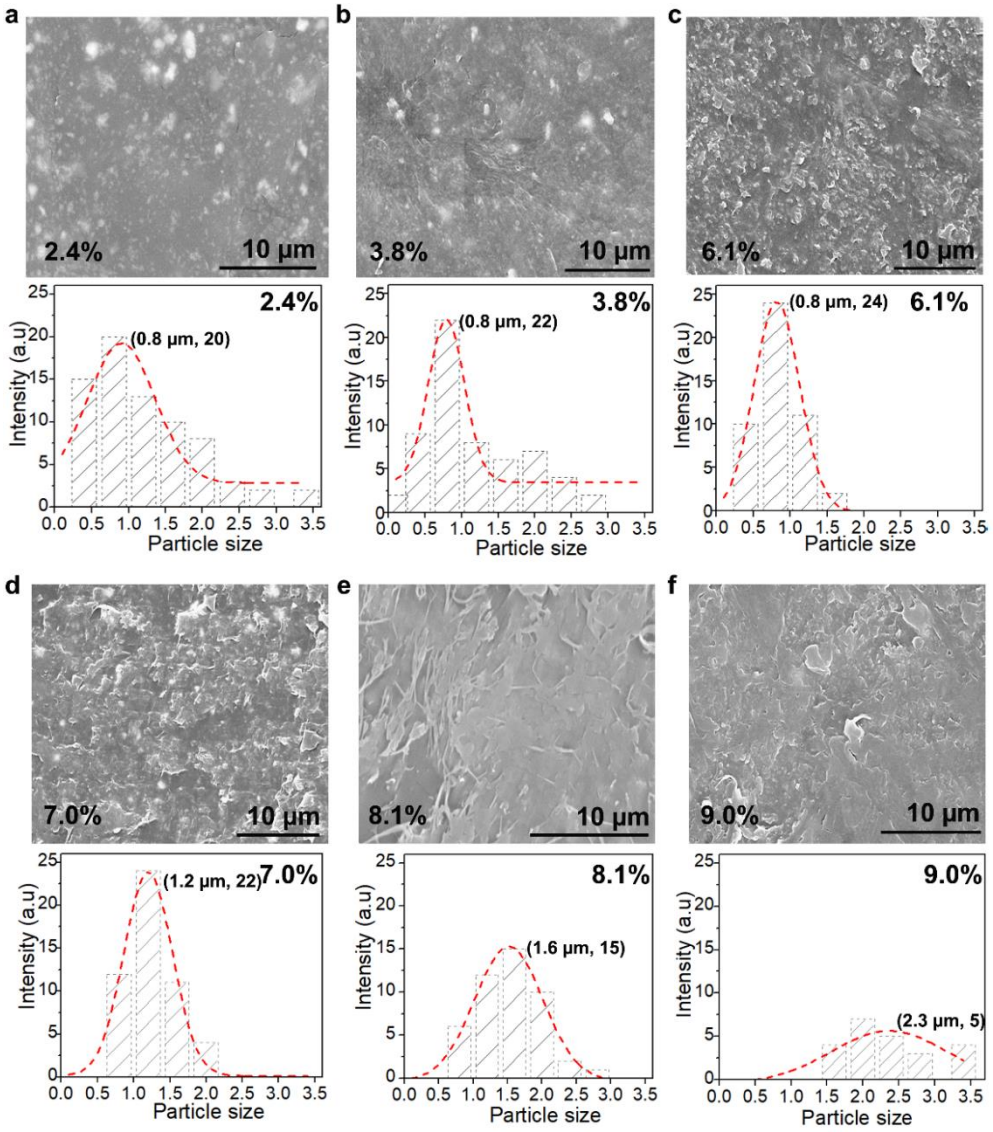

Fig. 3-2. The surface morphology and ZnO NP (4%) size distributions of the films dissolved in the different mass fractions of LDPE. a) 2.4 wt%, b) 3.8 wt%, c) 6.10 wt%, d) 7.0 wt%, e) 8.1 wt%, and f) 9.0 wt% of LDPE in xylene.

3.1.4 Effects of duration on the solubility of LDPE and dispersion of NPs

In the process of mixing polymer and NPs, it is necessary to completely dissolve the polymer in the solution. Thus, the polymer solution has to be stirred long enough at a sufficient temperature to increase the entropy, according to Equation 3-1. To determine the proper dissolution time, a solution with 4 wt% of ZnO/LDPE and 3.2% of LDPE/xylene was prepared in 105 °C oil bath and stirred for different hours to produce the casted films (see Group 3 in Table 2). The left column of Fig. 3-3 presents the states of the casted films after dissolution for 90, 120, 188, 202, and 322 h, respectively. The casted film dissolved for 90 h has large, isolated blocks (**Fig. 3-3.** a). As the duration increased, the areas of the isolated blocks become flatter and larger first (120 h) and then gradually formed larger number of smaller blocks (188 h), which started to merge into larger and more continuous pieces (202 h) until finally forming a whole smooth piece (322 h). The middle and right columns of Fig. 3-3 present the SEM images and size distributions, respectively, of NPs in the hot-pressed films corresponding to the casted films for various dissolution hours. In the SEM images, the NP clusters were identified, and their sizes and numbers were measured. The particle agglomerate sizes became smaller and smaller as the dissolution time was prolonged until the peak particle or cluster sizes (60 nm for the 322-h group) reached that close to the individual particle size (90 nm), as presented in the right column of Fig. 3-3.

Another way of determining the degree of NP dispersion in LDPE is the measurement of the transmissivity of the film to thermal radiation. In principle, the transmissivity of

incident light can be reduced by either Rayleigh scattering or Mie scattering which is dependent on the particle sizes [10]. Rayleigh scattering occurs due to the existence of particles with a size parameter $X \ll 1$, calculated as follows [11]:

$$X = 2\pi r/\lambda \qquad (3\text{-}3)$$

where r denotes the spherical particle radius, and λ denotes the wavelength of incident light. According to this principle, particles with diameters of 90–120 nm are suitable for the preparation of a transparent radiative cooling film with Rayleigh scattering. In this study, the NPs utilized had an average diameter of 90 nm, which could have strong Rayleigh scattering, thus ensuring good shielding against radiation in the UV region (10-400 nm) if dispersed well. Fig. 3-3 f presents the transmissivities of the films for thermal radiation. For the films formed with 90-h and 122-h dissolution times, the transmissivities for thermal radiation were high in the whole wavelength range. For the films formed with 188-h dissolution time, the transmissivity of radiation below 400-nm wavelength was substantially reduced, whereas that for the films with 202-h dissolution time was further suppressed significantly. For the films with 322-h dissolution time, the thermal radiation in the UV range was almost completely blocked. This result corresponds well to the particle size reduction pattern. In summary, as the dissolution time increased, the bonding force between NPs in an agglomerate could be diminished by continuously increased entropy provided by the solution system, resulting in reduced agglomerate sizes, which reported in Jancar et al article [12]. Consequently, the film became more effective in shielding the light, especially in the UV region. This indicates that the film with good NP dispersion could

have good spectrum selective properties and thus promising passive cooling performance as passive cooling materials.

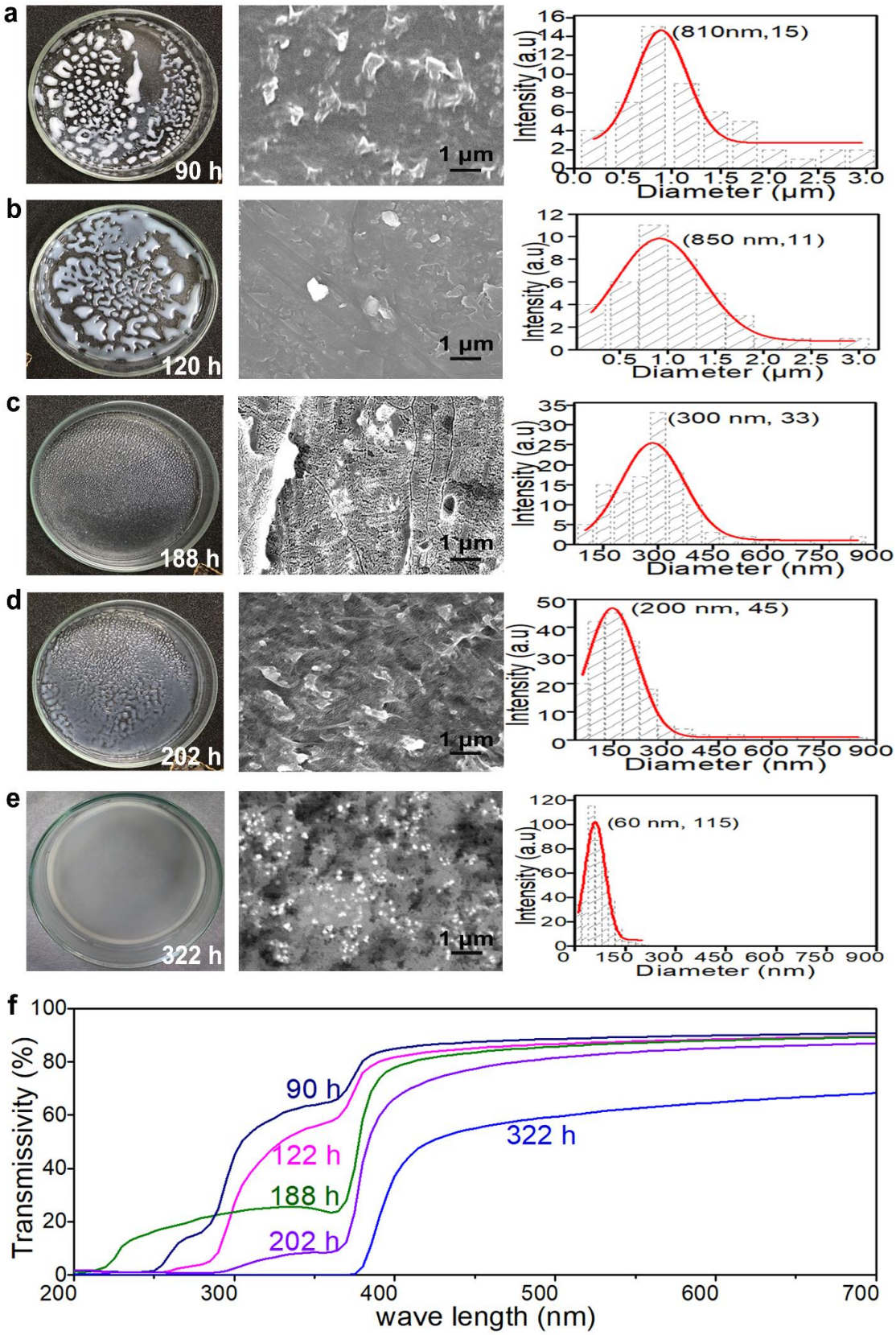

Fig. 3-3. Effect of dissolution time on ZnO NP dispersion in LDPE. a-e) The left column presents the ZnO/LDPE casted films, the middle column presents the SEM images of the

hot-pressed ZnO/LDPE films, and the right column presents the corresponding particle size distributions. f) The transmissivity curves of the ZnO/LDPE films after the different dissolution times.

3.2 Mechanism of the effect of dissolution time on NP dispersion

The mechanism for the effect of dissolution time on NP dispersion may be explained using **Fig. 3-4**. Polymer dissolution and NP dispersion are the two partially overlapping but somewhat consecutive processes in casting a homogeneous ZnO NP-doped LDPE film. The former must occur first for the latter to proceed. In the beginning of the dissolution, the polymer molecules formed clusters of about 1-mm diameter (according to our visual observation), which originated from the pellets of solid polymer before dissolution. And the NPs agglomerated into clusters of about 0.8-μm diameter, which contain hundreds of NPs (Fig. 3-4. a) due to initial mechanical blending and mixing. The polymer clusters were from the melting and dissolution of the semi-crystalline polymer pieces. In such a relatively high concentrated polymer solution, polymeric molecular entanglement is inevitable. These entangled chains can be gradually stretched at a high temperature in a proper solvent. Moreover, polymer molecular chains can diffuse toward low-concentration regions or boundaries between the polymer clusters, although this process could be very slow due to the high viscosity of the solution. In the current study, the films casted after the dissolution time of 202 h or longer could form a relatively complete film. This indicates that LDPE chains in the neighboring clusters reached out or diffused out to bridge or bond the clusters together to form a more homogeneous film. In addition, the diffusion of polymer molecular chains toward the boundaries could effectively create larger intermolecular distance

between the polymer molecules near the NP agglomerates and thus accelerate the diffusion of the NPs into the polymeric gel. Only after that could the ideal dispersion of the NPs be fulfilled. In this study, the ideal NP dispersion was achieved in 322 h. Vigneshwaran et al. dispersed surface treated 40 nm ZnO NPs in HDPE and shielded about 65% of UV because the NPs agglomerated into about 1 μm clusters [13]. Xiong et al. reported that total UV-shielding could be achieved with NP concentration higher than 7wt% in a ZnO/ poly(styrene butylacrylate) latex composite film [14], while 4wt% was sufficient for complete shielding of UV in the current study. Obviously, the performance of our ZnO/LDPE composite films is better than those reported in literature.

As the polymer cluster started to dissolve at 188 h, the NPs began to diffuse into the polymer, and the agglomerates started to diminish [12]. The dispersion of the agglomerated NPs in the polymer solution is determined by two factors, namely, the van der Waals forces holding the NPs together and the Brownian motion for the diffusion of the NPs to move toward the direction of lower particle concentration [15]. The diffusion coefficient, *D*, for spherical NPs can be calculated using the Stokes–Einstein equation [16]:

$$D = \frac{kT}{3\pi\mu d} \qquad (3\text{-}4)$$

where *k* denotes the Boltzmann constant; *T*, the temperature in Kelvin; μ, the viscosity of the polymer solution; and *d*, the particle diameter. As the NPs in the agglomerated clusters diffuse toward the polymer matrix due to the Brownian motion, the diffusion rate relates positively to the temperature and negatively to the polymer solution viscosity and the particle diameter. Cui et al also interpreted the dispersion of NPs in the liquid-liquid

interface, like a transition from diffusive to confined dynamics was manifested by intermittent dynamics [17]. In the current study, we have quite small NPs (90 nm) and quite high concentration of LDPE (3.2%), which results in slow NP diffusion. Consequently, good dispersion was only achieved after quite a long dissolution time (322 h) at an elevated temperature.

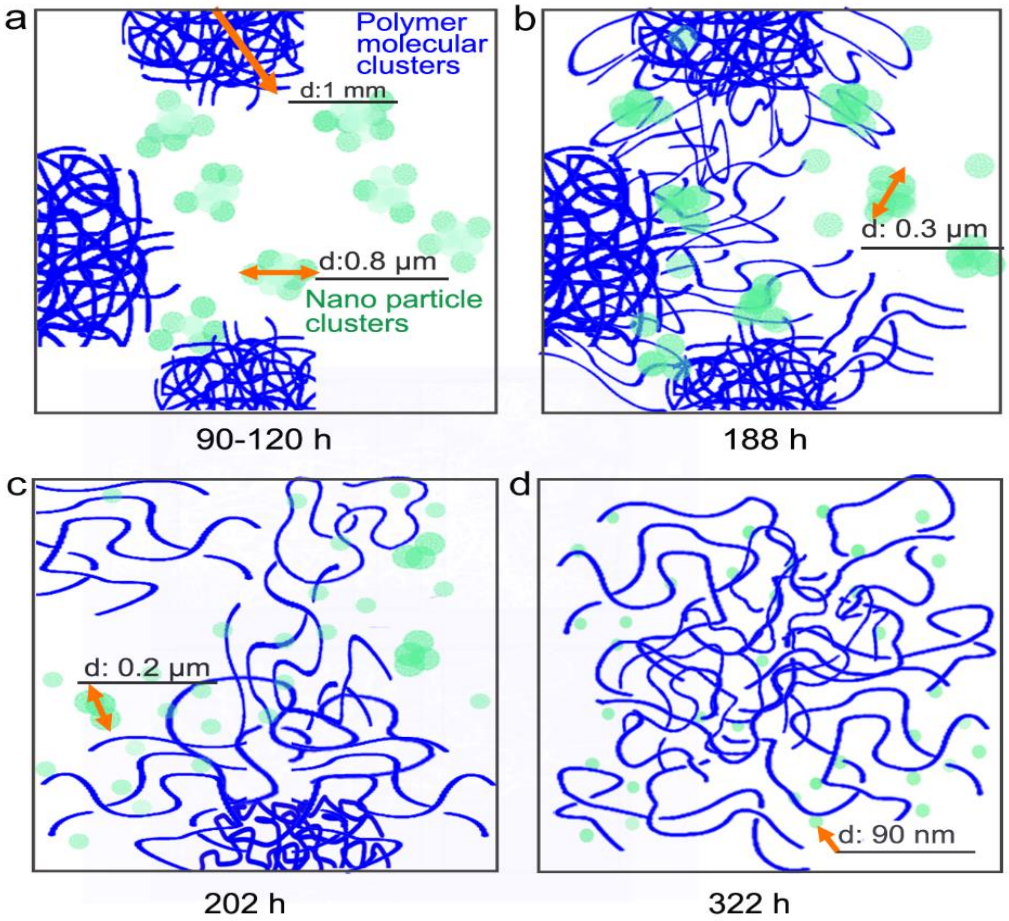

Fig. 3-4. The mechanism of uniformly mixing LDPE and NPs governed by time, temperature and concentration of LDPE and NPs.

Of course, the dissolution time in the current study is not necessarily optimal because some other factors such as dissolution temperature and LDPE concentration could greatly influence the process. According to Equation 1, when temperature increases, ΔG will be decreased and thus stretching out of polymer chains would be more preferable leading to a shorter optimal dissolution time in addition to the increased diffusion coefficient discussed above. Lowering the LDPE concentration could also facilitate diffusion process for both the polymer and the NPs since it could greatly reduce the viscosity of the solution, leading to a reduced dissolution time.

3.3 Optimizing the Transmissivity of Spectrum Selective Film

3.3.1 Size of NP effect on the transmissivity of spectrum selective films

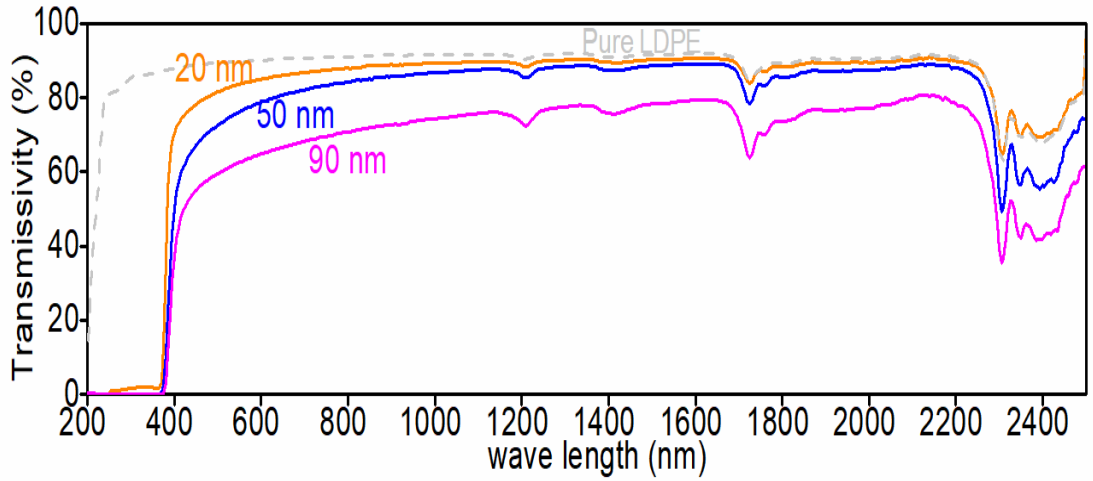

Fig. 3-5. Size of NPs effect on the transmissivity of spectrum selective films.

The transmissivity of spectrum selective films is affected by the nanoparticles' size dispersed in (experimental conditions showed in group 1 of Table 2-3), as the light scattering effect changes with the size parameter X of nanoparticles, ($X = 2\pi r/\lambda$, r is the spherical particle radius, and λ is the wavelength of incident light). The three curves in color (shown in **Fig. 3-5**) are the transmissivity of films dispersed 4 wt% ZnO NPs with diameter of 20 nm, 50 nm and 90 nm, respectively, with thickness of 0.12 ± 0.05 mm. It is shown that the shielding effects of the three films are similar in UV light region. While in the transition region from UV to Vis region (380 - 420 nm), the trend of film transmissivity

moves to the right and downward as the size of nano particle increases. In Vis spectrum region (400 – 700 nm), the transmission gradually decreased with diameter of NP increased. And the transmissivity curves of films with different size of nanoparticle in the nIR region (700 - 2500 nm) like parallels to the transmissivity of pure LDPE curve, but each distance between the transmissivity of samples and that of pure LDPE became larger as the size of doped NP increased.

3.3.2 Concentration of NP effect on the transmissivity of spectrum selective films

The transmissivity of membranes is also influenced by the concentration of NP (Fig. 3-6. a). Films doped with 4%, 5%, and 6% ZnO NPs were tested to determine the effect of particle concentration on the transmissivity of the films. The transmission of films with thickness of 0.12±0.05 mm increased as the concentration of NP decreased especially in Vise lights region. Also, each distance between the transmissivity of samples and that of pure LDPE get closer as the wavelength of incident light changing from 400 nm to 1700 nm. While if the incident light wavelength located in 2200 nm to 2500 nm, the transmissivity curves of samples almost overlapped as one curve. That means as the wavelength of incident light increase, the scattering effect on incident light by NP with diameter of 90 nm is from strong to weak. And an estimate that the influence of NP was neglectable when the incident wavelength is longer than 2500 nm.

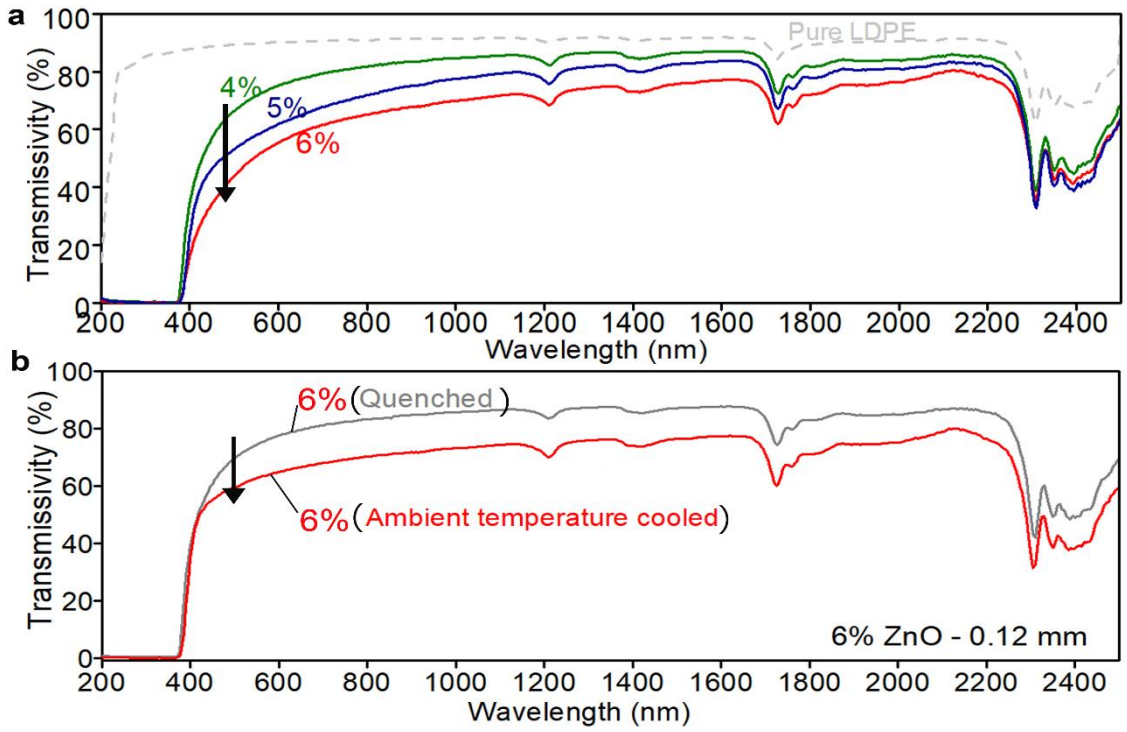

Fig. 3-6. The factors affecting the transmissivity of composite films. a) Effect of the nanoparticle concentration, b) effect of film crystallinity treated by different hot post curing processes.

3.3.3 Crystallinity of film effect on the transmissivity

The transmissivity of spectrum selective film is closely related to the crystallinity of itself. The crystallinity of membrane is decided by the processing methods after hot press the casting film. **Fig. 3-6.** b showed the transmissivity of 2 spectrum selective ZnO/LDPE films treated either by processing of quenching or ambient temperature cooling after hot press. The curves in color are the samples treated by quenching process (from 120 ℃ to an ice-water bath of 0 ℃), and that in gray were samples cooled by ambient temperature (samples were cooled naturally from 120 ℃ to ambient temperature 25 ℃ in the hot press machine).

The transmissivities of each group are different in visible region and almost in the same level in ultraviolet region.

3.3.4 Thermal properties of spectrum selective transparent films

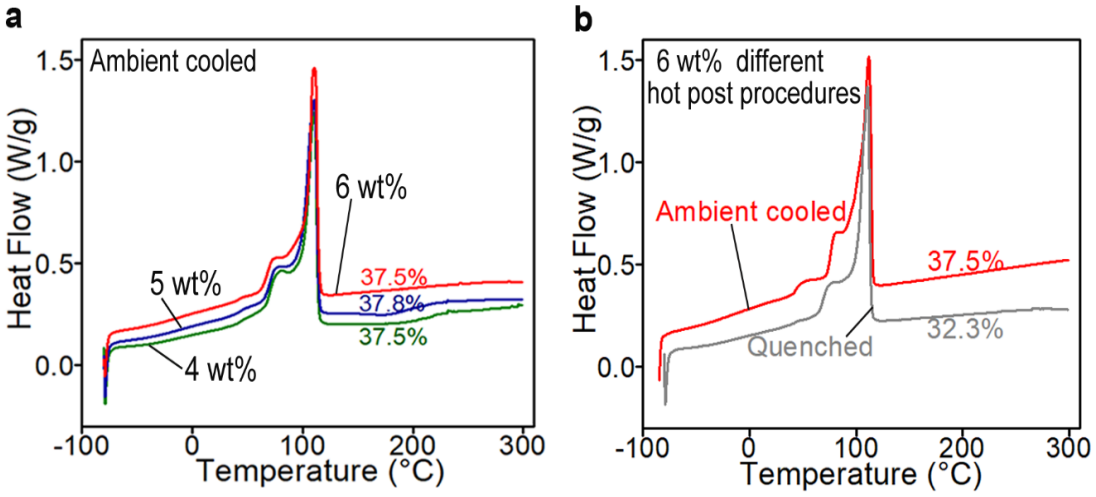

Fig. 3-7. Thermal properties of spentrum selective transparent films. a. the DSC curves of films under the ambient cooling hot post process with size of 90 nm and different particle concentrations of 4wt%, 5wt% and 6wt%; b. the DSC curves of different hot post procedures of quenched and ambient temperature-cooled samples with 6 wt% of 90 nm NPs doped.

Thermal properties of the films were determined using deferential scanning calorimetry (DSC) in nitrogen on a machine Model CCTA DSC25. The specimens were equilibrated at -80 °C for 2 min and then heated at 10 °C/min to 300 °C at which they were isothermal for 2 min, and then cooled down at 10 °C/min to -80.00 °C.

The transmissivity of the films is closely related to the crystallinity of the film [18], especially in the Vis region. And the crystallinity of the spectrum selective transparent ZnO/LDPE film is determined by the hot post procedures of the casted film. **Fig. 3-7** presented the DSC curves of samples which were treated with different hot post procedures either quenched or cooled at an ambient temperature. The DSC curves revealed that the crystallinity of the quenched film was substantially lower than that cooled at an ambient temperature. Jordan with coworkers described the crystallinity in different processing influenced by temperature [19]. In general, a quenched film is likely to have smaller crystals and lower crystallinity due to a much shorter time for the crystals to grow, thus leading to high transmissivity compared with an ambient temperature-cooled film.

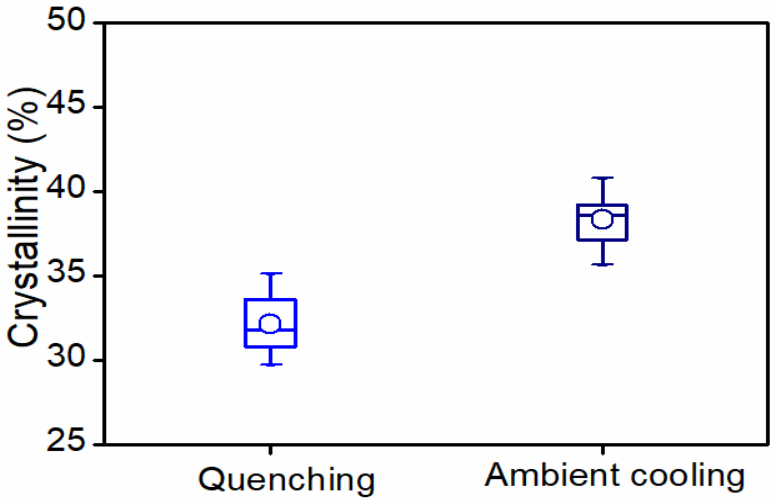

Fig. 3-8. The crystallinity distribution treated with different hot post procedures (quenched or cooling by ambient temperature) of spectrum selective transparent ZnO/LDPE films.

Figure. 3-8 showed the crystallinity distribution of two groups, for each of which was

22 samples were either treated by quenching or ambient temperature cooling post processing after hot press. The average crystallinity of quenching film was 32.1%, while that of ambient temperature cooling was around 38.5%.

3.4 Mechanical Performance of Films

The mechanical property of the films is presented in **Fig. 3-9** and **Table 3-1**. The failure strains of the NP-doped films decreased from 98% to 78% with an increase NP size from 20 nm to 90 nm. The failure strains of the NP-doped films decreased from 80% to 8% with an increase in the NP concentration from 4 wt% to 6 wt%, respectively. the failure stress were decreased from 15 MPa to 5MPa because of quenching process of samples in Fig. 9. c. Conversely, the tensile strength increased with the increase in the NP concentration which reported by Wang et al [1]. It seems that the mechanical properties of the films changed from being typical ductile materials to relatively brittle materials due to failure mechanism change from localized plastic deformation to defects dominant brittle failure. This could be observed in SEM images (see Fig. 3-10) of the films which show as the NP concentration increased, the distance between neighboring NPs is decreasing drastically and thus could possibly increase probability of containing weak spots in the specimen. On the other hand, the tensile strength and failure strain of the film were much lower for the quenched film compared with the film cooled at an ambient temperature due to creases or nano-cracks generated by quenching on the surface of the quenched film as shown in Fig. 3-10.

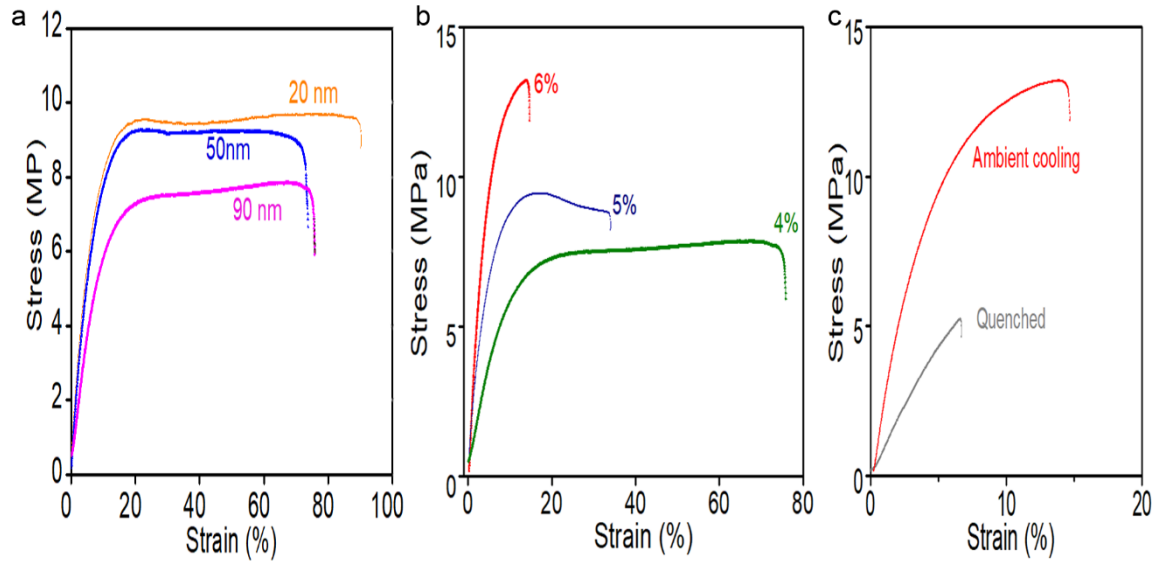

Fig. 3-9. The stress–strain curves of ZnO/LDPE films with thickness 0.12 ± 0.05 mm. a) Films doped with diameters of 20 nm, 50 nm, 90 nm particles with 4wt% concentrations of ZnO NPs, b) films doped with 4wt%, 5wt%, and 6wt% concentrations of 90 nm ZnO NPs, c) films doped with 6wt% concentrations of 90 nm ZnO NPs which were post hot-pressed by quenching or ambient temperature cooling. All

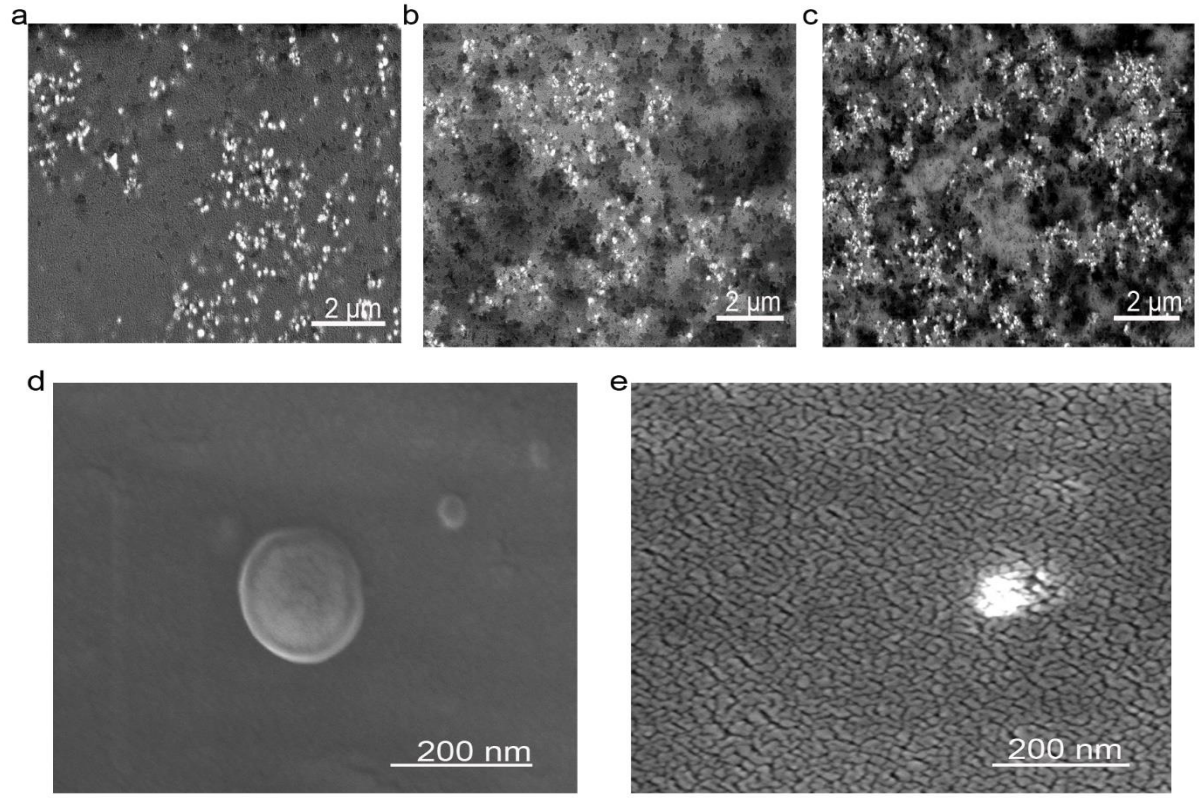

Fig 3-10. SEM images of the ZnO-LDPE films doped with 90 nm particles. a) 4% ZnO NP; b) 5% ZnO NP; c) 6% ZnO NP; d) the high magnification of 6% ZnO NP film cooled with ambient temperature of post hot press; e) 6% ZnO NP film quenched of post hot press.

Table 3-1. Mechanical properties of passive cooling films

Samples	Particle size (nm)	Weight percentage (wt%)	Post procedure	Tensile stress (MP)	Young's modulus (MP)	Failure strain (%)
1	20 [c]	4	Am[a]	9.3	2.88	100
2	50	4	Am	9.2	1.8	78.8
3	90	4 [d]	Am	7.6	5.4	79.3
4	90	5	Am	9.7	2.3	29.6
5	90	6	Am [e]	10.8	3.9	7.3
6	90	6	Qu[b]	5.1	1.5	6.9

[a] Samples treated by ambient cooled post-processing;

[b] Samples treated by quenched post-processing;

[c] Group of Fig 3-8. (corresponding conditions shown in group 1 of Table 2-3);

[d] Group of Fig 3-8. (corresponding conditions shown in group 2 of Table 2-3);

[e] Group of Fig 3-8. (corresponding conditions shown in group 1 of Table 2-3).

3.5 Conclusions

To make a spectrum selective or UV-shielding ZnO NP-doped film with uniform dispersion of the NPs and ideal transmissivity for spectrum tailoring, a systematic study was conducted to determine the critical parameters for film fabrication (e.g., casting temperature, polymer concentration, and dissolution time). It was found that the casting temperature has to be maintained at 115 °C or above in vacuum to ensure the formation of a transparent and uniform film without oxidation. For proper initial dispersion of the NPs in the polymer solution, the LDPE concentration should be lower than 6%. For a uniform and complete dispersion of individual NPs, the dissolution time has to be sufficiently long for the polymer molecules to unentangle first, which could allow the diffusion of the NPs into the polymer gel, thus resulting in a homogeneous NP dispersion. Only when the NPs are well dispersed will the film have ideal shielding against UV light while allowing a reasonable amount of visible light to be transmitted. The transmissivity of the films can be optimized by changing the concentration of doped NP and the crystallinity of the film through quenching. The mechanical properties of the UV-shielding films were altered from ductile to brittle by varying the NP concentrations.

References

[1] M.M. Sebastian Koltzenburg, Oskar Nuyken, Polymer Chemistry, Springer, New York, 2017.

[2] A. Ali, E.Y. Hwang, J. Choo, D.W. Lim, Nanoscale graphene oxide-induced metallic nanoparticle clustering for surface-enhanced Raman scattering-based IgG detection, Sensors Actuators B: Chem. 255 (2018) 183-192. https://doi.10.1016/j.snb.2017.07.140.

[3] L. Mu, J. He, Y. Li, T. Ji, N. Mehra, Y. Shi, J. Zhu, Molecular Origin of Efficient Phonon Transfer in Modulated Polymer Blends: Effect of Hydrogen Bonding on Polymer Coil Size and Assembled Microstructure, J Phys Chem C 121(26) (2017) 14204-14212. https://doi.10.1021/acs.jpcc.7b03726.

[4] N.R. Choudhury, R. Vilaplana, R. Botet, A.K. Sen, Comparison of light scattering properties of porous dust particle with connected and unconnected dipoles, Planet and Space Sci 190 (2020). https://doi.10.1016/j.pss.2020.104974.

[5] A.H. Hsieh, D.S. Corti, E.I. Franses, Rayleigh and Rayleigh-Debye-Gans light scattering intensities and spetroturbidimetry of dispersions of unilamellar vesicles and multilamellar liposomes, J. Colloid Interface Sci. 578 (2020) 471-483. https://doi.10.1016/j.jcis.2020.05.085.

[6] J. Jancar, F. Ondreas, P. Lepcio, M. Zboncak, K. Zarybnicka, Mechanical properties of glassy polymers with controlled NP spatial organization, Polym. Test. 90 (2020) 106640-106649. https://doi.10.1016/j.polymertesting.2020.106640.

[7] B.W. Mansel, C.-Y. Chen, J.-M. Lin, Y.-S. Huang, Y.-C. Lin, H.-L. Chen, Hierarchical Structure and Dynamics of a Polymer/Nanoparticle Hybrid Displaying Attractive Polymer-

Particle Interaction, Macromolecules 52(22) (2019) 8741-8750. https://doi.10.1021/acs.macromol.9b01141.

[8] N. Shokeen, C. Issa, A. Mukhopadhyay, Comparison of nanoparticle diffusion using fluorescence correlation spectroscopy and differential dynamic microscopy within concentrated polymer solutions, Appl. Phys. Lett. 111(26) (2017). https://doi.10.1063/1.5016062.

[9] M. Cui, C. Miesch, I. Kosif, H. Nie, P.Y. Kim, H. Kim, T. Emrick, T.P. Russell, Transition in Dynamics as Nanoparticles Jam at the Liquid/Liquid Interface, Nano Lett. 17(11) (2017) 6855-6862. https://doi.10.1021/acs.nanolett.7b03159.

[10] J.M. Lagarón, A. López-Rubio, M. José Fabra, Poly(L-lactide)/ZnO nanocomposites as efficient UV-shielding coatings for packaging applications, J. Appl. Polym. Sci. 133(2) (2016) 42426-42433. https://doi.10.1002/app.42971.

[11] A.M. Jordan, K. Kim, D. Soetrisno, J. Hannah, F.S. Bates, S.A. Jaffer, O. Lhost, C.W. Macosko, Role of Crystallization on Polyolefin Interfaces: An Improved Outlook for Polyolefin Blends, Macromolecules 51(7) (2018) 2506-2516. https://doi.10.1021/acs.macromol.8b00206.

[12] X. Wang, P. Xu, R. Han, J. Ren, L. Li, N. Han, F. Xing, J. Zhu, A review on the mechanical properties for thin film and block structure characterised by using nanoscratch test, Nanotechnol Rev 8(1) (2019) 628-644. https://doi.10.1515/ntrev-2019-0055.

Chapter 4　Passive cooling performances of spectrum selective film

Chapter 4 Passive cooling performances of spectrum selective films

4.1 Introduction

The two largest energy consumption sectors are buildings and transportation, which consume approximately 40% [1] and 23% [2] of global energy, respectively. Temperature regulation for buildings [3] and automobiles with window systems consumes 60% [2] and 23 to 41% [4, 5] of the total energy expenditure, respectively, which leads to excessive greenhouse gas emissions [6-9]. Since regular air conditioning requires high energy consumption, new approaches for cooling have been attempted in recent years. One of these approaches is passive radiative cooling for both indoor and outdoor environment, which does not involve any energy input [10, 11]. Passive cooling is often achieved using films that block solar irradiance or highly transmit mid-IR light [11-24]. However, almost all films developed thus far are either opaque and/or involve complicated manufacturing processes and application procedures. For example, in passive cooling of buildings, most solar control films are made of layered materials with a thermal emitter and a solar reflector based on the photonic properties of coated materials [25]. In the cooling of automobile cabins, films or coatings for smart windows are generally made of electro-, photovoltaic [4], and thermal chromatic materials triggered by an electric voltage or a predesignated temperature at which near-IR (800–2500 nm) is reflected to reduce IR irradiation, in addition to shielding UV light. These

mechanisms require additional energy for monitoring and have complicated control systems.

Little has been reported about translucent or transparent cooling films made of nanoparticles (NPs) and polymers. Fan et al. reported a 4.6 °C reduction using a translucent radiative cooling film made from fluorinated polyimide (PI) coated with SiO_2 microspheres and a silver layer [22]. However, PI films are not generally suitable for cost-sensitive automobiles and office buildings. Passive-cooling films currently used in buildings and automobiles are expensive in terms of raw material cost and manufacturing processes, with rather limited temperature reduction performance. Another problem with materials used for existing passive-cooling films is that they have all been evaluated using self-made experimental setups with largely different designs [16, 18, 20, 26, 27], making comparisons of results difficult. One of the major issues is that the efficacy of the passive-cooling materials has been evaluated in such a way that insufficient information is provided about the relationship between temperature reduction and the volume of air influenced by the cooling material. Targeting these problems, we have developed an affordable and scalable spectral-selective transparent passive-cooling film and a testing device with adjustable volumes for evaluating te cooling effect of solar radiation filter materials.

4.2 Experimental section

4.2.1 Principles for material selection.

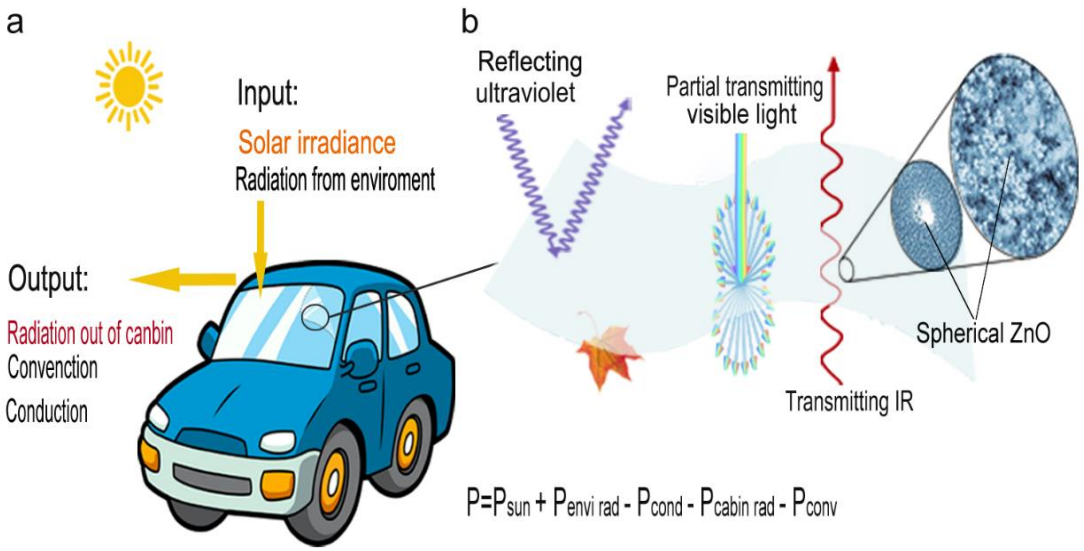

Fig. 4-1. Schematics illustrating. a) heat sources for an exposed car under solar radiation and b) the principle of passive-cooling films through selective shielding of solar radiation and transmittance of thermal radiation emitted by heated objects inside a car.

Fig. 4-1. a and b illustrate how thermal energy is exchanged for a passenger car and the principle of scattering mechanism of an ideal passive cooling film. As indicated in Fig. 1, the temperature change in a parked car exposed directly under solar irradiation relies on total energy, P, the summation of the energies expressed as:

$$P = P_{Sun} + P_{envi\,rad} - P_{cond} - P_{Cabin\,rad} - P_{conv} \qquad (4\text{-}1)$$

where P_{sun}, $P_{envi\ rad}$, P_{cond}, $P_{cabin\text{-}rad}$, and P_{conv} are the energies obtained from solar irradiation,

environmental radiation, thermal conduction, irradiation from inside the cabin, and thermal convection, respectively. The goal is to fabricate a film that can block the high energy region of the solar irradiation of P_{sun} while allowing the passage of the thermal radiation from the cabin, $P_{cabin\text{-}rad}$.

The idea is to use a film which can block the high-energy portion of solar irradiation while allowing the passage of thermal radiation from the automobile cabin. Therefore, in this study, films made of spherical ZnO NPs dispersed in LDPE were fabricated to selectively shield or transport targeted wavelengths in all thermal radiation spectra (0.1–16 μm) [28]. Although LDPE has narrow characteristic absorption peaks in the IR region, each peak has negligible energy absorption compared with the energy transported through the material (**Fig. 4-2**). ZnO has a high refractive index of $n \approx 2.0041$ [29] and its characteristic peaks are mostly located in the UV region, except for a few small absorption peaks in the Vis region ($\lambda > 400$ nm wavelength) up to the near-IR (nIR, 0.8 nm $< \lambda <$ 2.5 nm) and mid-IR region ($\lambda < 16$ μm wavelength). In addition, light can also be blocked by either Rayleigh scattering or Mie scattering dependent on NP size [30]. As shown in the **Fig. 4-3 and Fig. 4-4**, the incident light scattering effect occurs due to the existence of ZnO NPs with sizes meeting the requirement of the particle size parameter X in the range of 10^{-1} to 10^{2}. The size parameter is calculated as [30]:

$$X = 2\pi r/\lambda \qquad (4\text{-}2)$$

where r is the spherical particle radius and λ is the incident light wavelength. According to this principle, NPs with diameters of 90 nm will have X = 0.71–1.41 in the UV wavelength range of 200–400 nm, which could generate strong scattering suitable for preparing a transparent passive-cooling film. This ensures shielding of a large portion of higher energy photons and a small fraction of lower energy photons of the visible light.

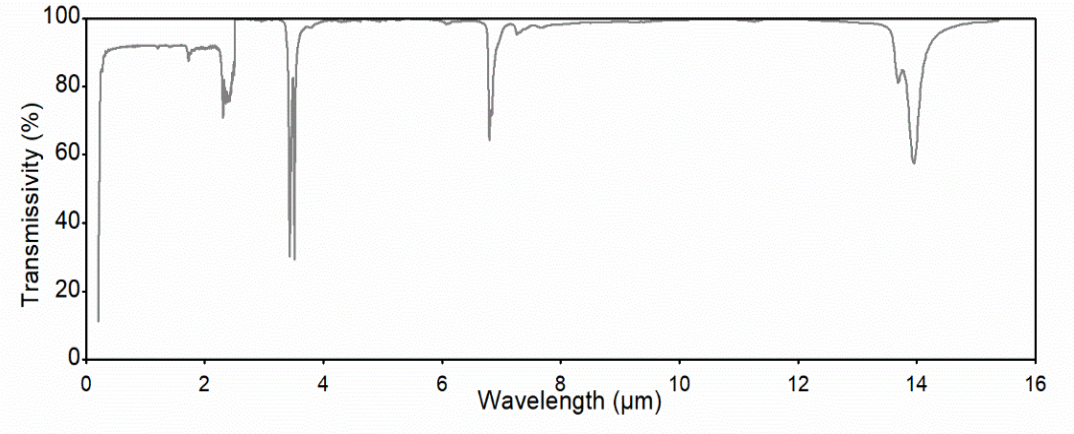

Fig. 4-2. Characteristic absorption peaks of pure LDPE.

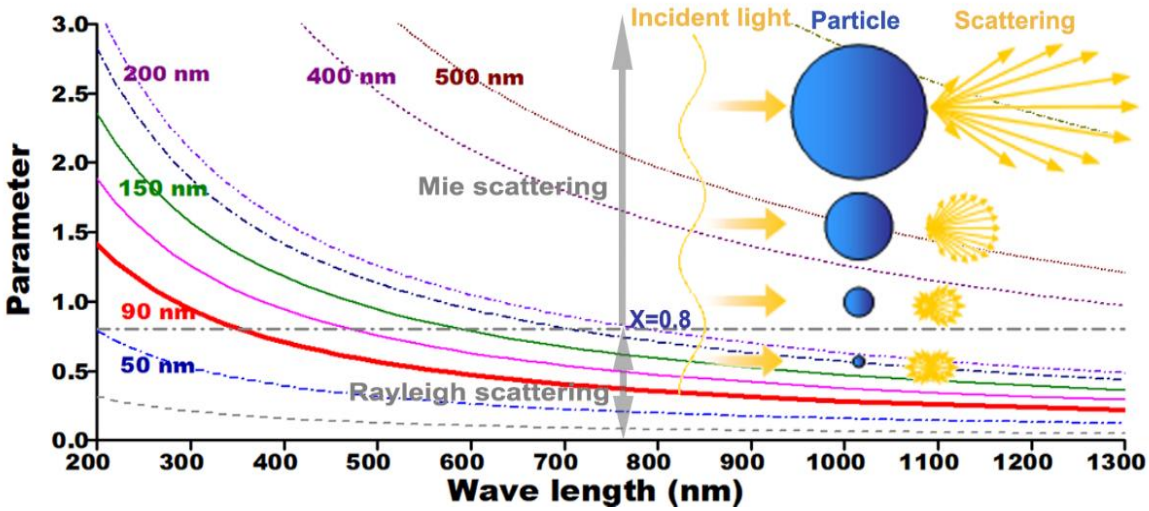

Fig. 4-3. Relation between the particle size parameter and scattering mechanisms

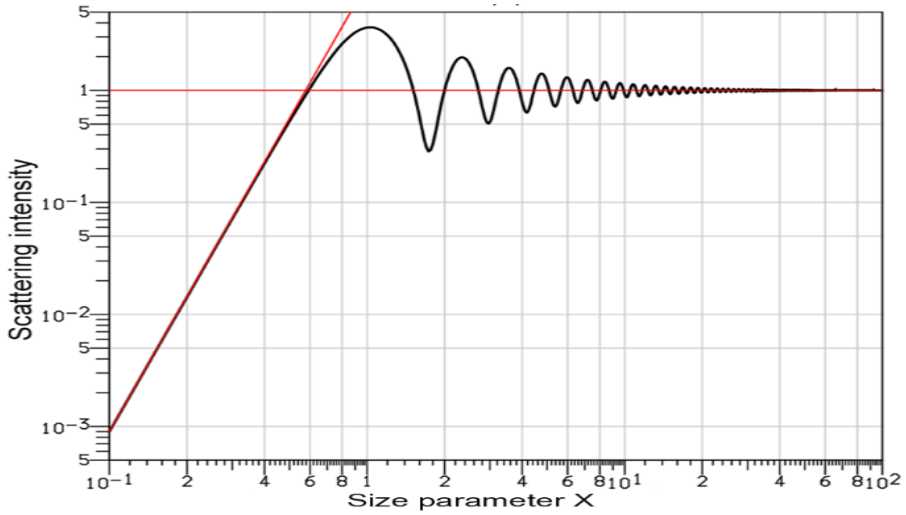

Fig. 4-4. Scattering effect intensity versus size parameter X. NPs with diameters of 90 nm have X = 0.71–1.41 in the UV wavelength range of 200–400 nm, which generates the strongest scattering effect.

However, mixing NPs with molten polymers is always difficult since there is too large of a surface area to wet. This is perhaps why most published studies have used particles with diameters larger than 500 nm [20] or agglomerated smaller particles [31]. However, large particle sizes or agglomerated NPs pose two problems, namely, low transparency and poor mechanical properties. Large particles block Vis light because the sizes of the particles are in the same range of the Vis wavelength (380–780 nm). They are also likely to greatly influence fiber or film strength due to their size approaching 5–10% of regular fiber diameters (10–20 μm) or thin film thickness, leading to difficulties in processing and maintaining consistency of products. ZnO NPs have certain electromagnetic wave absorption properties [32], as well as photocatalytic effects for photodegradation by generating radicals or stabilization by the anti-photo-oxidation of LDPE, depending on which effect is more dominant. However, according to Kamalian et al. [33], the photodegradation process is relatively slow (5% weight and 10% tensile strength

reduction after 200 h exposure to noon-time UV irradiation). This is partially due to the UV shielding effect of ZnO NPs in the first few micro-meters of the composite film [34]. Therefore, composite films may last longer than their intended service time, after which the photocatalytic effect of ZnO could facilitate degradation of the LDPE film and reduce the environmental impact due to plastic waste. ZnO NPs could also be a catalyst for photodegradation of indoor pollutants, which could be highly beneficial for improving indoor air quality [35, 36].

Therefore, in this study, ZnO particles with 90-nm-average-diameters were mixed with LDPE in xylene at 110 ºC for about 300 h to form a well dispersed homogenous solution. The long time necessary for mixing is a result of the incompatibility of the NPs with LDPE and the high viscosity of the solution, which is a production problem. However, one may greatly shorten the mixing time by applying a surface treatment to the NPs to improve compatibility between NPs and LDPE. Additionally, using more dilute solution and/or a higher mixing temperature could reduce the viscosity of the solution. After mixing, the solvent was evaporated to form films that were subsequently hot-pressed into films with different thicknesses corresponding to different pressures. The crystallinity of films was altered through either cooling slowly in ambient temperature (for approximately 4 h) or quenching in an icy water bath (details are in the Supplementary materials). A series of tests were carried out to determine the properties and performance of the ZnO-doped LDPE films, furthermore, referred to as the ZnO/LDPE film. Further film preparation details and test-setup information can be found in the Supplementary materials.

4.2.2 Preparation and characterizations of the films

LDPE pellets (AS: 9002-88-4) with a melting index of 25 g/10 min were purchased from Alorich Chemistry. ZnO NPs with an average diameter of 90 nm were provided by Rhawn Company in Shanghai, China. The particles were first dispersed in xylene for 20 min and then LDPE pellets were added and dissolved in the dispersion solution in an oil bath at 110 ℃, with magnetic stirring. ZnO, LDPE, and xylene were mixed at weight ratios of 0.042:1:50, 0.053:1:50, and 0.064:1:50, corresponding to samples with 4, 5, and 6% particle concentrations, respectively. The solvent was extracted in vacuum at 115 ℃ to form casted films. The films were hot pressed at 0.4, 0.7, 6, and 15 MPa in vacuum at 125 ℃ to fabricate transparent membranes with thicknesses of approximately 160, 140, 11, and 7 μm, respectively. The hot-pressed films were either cooled slowly in ambient temperature (about 4 h) or quenched in a 0 ℃ icy water bath. Figure 2a shows a hot-pressed film, under which our silver university logo can be clearly identified, and the particle-doped pellets ready for scaled-up blow-molding production of regular films.

Microscopy analysis

The surfaces of the films, corresponding elemental mapping, and analysis were examined with a field-emission scanning electron microscope (FE-SEM: Zeiss MERLIN, Oberkochen, Germany). The samples were sprayed with Au for 45s before imaging.

X-ray diffraction analysis

X-ray diffraction (XRD) was performed on the films using a MiniFlex 300 (Rigaku Corporation, Japan). The scan range was set between 10° and 80° and the scan rate was 0.04 °/s. The tube voltage and experimental current were 40 kV and 20 mA, respectively.

Transmittance test

The transmittance tests for the cooling films were performed using an ultraviolet–visible–near infrared (UV–vis–NIR) spectrometer (Yokogawa Model AQ6375B) and Fourier transform infrared (FTIR) spectrometer with integrating spheres (Model Nicolet iS50).

4.2.3 Passive cooling test

The passive-cooling test for the films was carried out in early autumn. The weather was relatively dry and mostly sunny. The daytime temperature was around 27–37 °C with a relative humidity (RH) around 45%. The films in the current study were mainly tested for the influence of thermal radiation such that thermal conduction and convection could be minimized. The testing system was designed using sealed boxes, each with a window, a temperature measurement system composed of a few sensors (semiconductor thermal sensor LM35 from Akizukidenshi Company, Japan), a data recorder (e-corder410 eDAQ Pty Ltd. Sydney, Australia), and a solar irradiance monitor (PG2000-pro scientific glass spectrometer and NIR2500 near IR spectrometer, Shanghai Ideaoptics Company, China).

The in-situ testing setup is shown in **Fig. 4-5.** a. A temperature sensor was placed 2-cm

below the window in the box to monitor and record the temperature change during the test (Figure 3b). Each sealed box had a volume of 13,734 cm^3 (23 × 37 × 16 cm) and a window of 70.88 cm^2 (r = 9.5 cm). The corresponding specific volume of the test device was 1.92 m. The box was made of polystyrene foam, lined with aluminum foil, and completely sealed to minimize heat transfer through conduction, convection, and secondary radiation from the outside in and the inside out. During the test, three identical boxes with windows were covered with either a piece of glass, designated as the control, or a piece of glass laminated with a radiation shielding cooling film with a thickness of 0.14 mm for particle concentrations of 4% and 6%, referred to 4% film and 6% film. The boxes were placed on a table 1.3-m above the ground to avoid heat transfer from the ground and were able to rotate to perpendicularly face the sun throughout the test. The system was exposed on a roof terrace for an entire day for a total of three clear days.

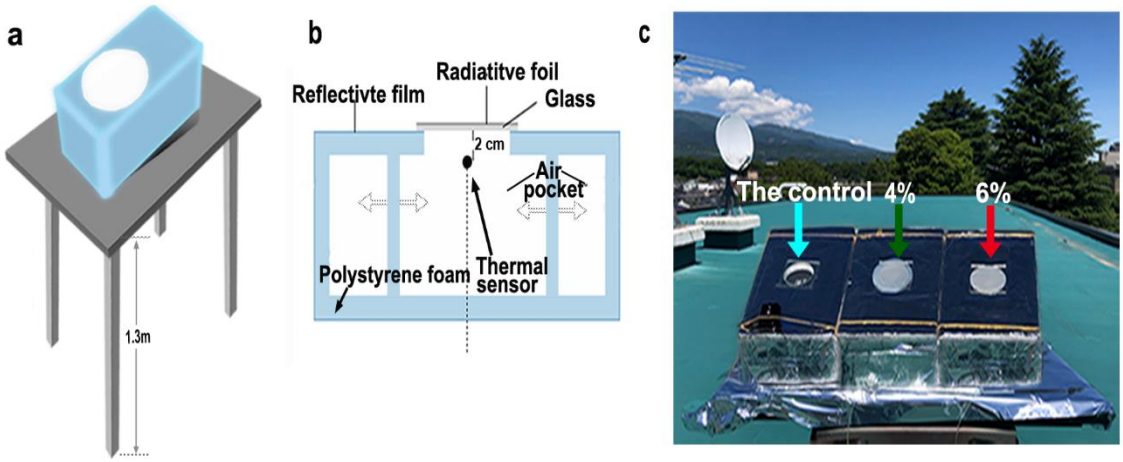

Fig. 4-5. Schematic of solar radiation test for passive cooling: a) The radiative cooling testing device, b) Arrangement in the testing box, c) In-situ testing setup.

The cooling power is an important performance parameter for these types of materials. It has

been deduced as the extinction of irradiance of the solar spectrum equal to the removal of light from its travel path due to both scattering and absorption effects of the spectrum-selective transparent film. To detect the relationship between the transmitted part of solar irradiance and the inner air temperature difference of the testing equipment, the transmitted region of the solar irradiance is the main source for heating the inner air temperature of the device. Assuming the thickness of the film is *s*, the intensity of solar radiance is $I_\lambda(s=0)$ and the intensity of solar light passing through the film is $I_\lambda(s=s)$. **Figure 4-6** illustrates the schematic of incident light transmitting through a passive-cooling film. The deduced process function is:

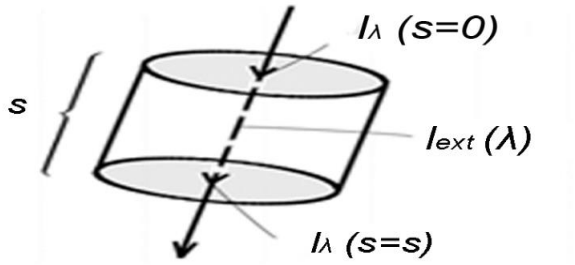

Fig. 4-6. Schematic of incident light transmitting through a passive-cooling film.

$$I_{\text{extinction}}(\lambda) = I_\lambda(s=0) - I_\lambda(s=s) = \int_{\lambda_0}^{\lambda_n} (I_\lambda(0) - I_\lambda(s))\, d\lambda \qquad (4\text{-}3)$$

For the control box, the heat mass balance of each moment is:

$$I_\lambda(l=0) * A = c * m * (T_1 - T_0) \qquad (4\text{-}4)$$

For the test box covered with by the film:

$$I_\lambda(l=s) * A = c * m * (T_2 - T_0) \qquad (4\text{-}5)$$

Therefore, the cooling power of the passive-cooling film is the ability to shield the solar irradiance:

$$P_{cooling} = I_{\text{extinction}} = (c * m * (T_1 - T_2))/A = (c * m * \Delta T)/A \qquad (4\text{-}6)$$

where $P_{cooling}$ is the cooling power, c is the specific heat of air, m is the air mass in the box, T_1 is the inner temperature of the control box, T_2 is the inner temperature of the box covered with sample, T_0 is the initial temperature before exposure to solar radiation, ΔT is the cooling

difference between the inner temperature of the control box (T_1) and the inner temperature of testing box covered with the film (T_2), and A is the window area of the testing box. The in-situ testing facility is shown in Fig 4-5. c.

4.3 Results and discussion

4.3.1 Characterization of the ZnO/LDPE film

Thin, transparent passive-cooling films and corresponding pellets for scalable production were also prepared (Fig. 4-7. a). The surface morphology of the films is shown in Fig. 4-7. b. The particle size dispersion in the film is shown in Fig. 4-8. FTIR data of samples were shown in Fig. 4-9. Elemental mapping and analysis information are shown in Fig. 4-10. a-b. Scanning electron microscopy (SEM) images and elemental mapping results show uniform distribution of ZnO NPs in the LDPE matrix. In addition, X-ray diffraction results, shown in Fig. 4-10. c indicate that the ZnO/LDPE film has almost exactly the same spectrum as that of the pure LDPE. This further indicates that the ZnO NPs are well dispersed in the polymer, as reported by Cheng and Yu [1].

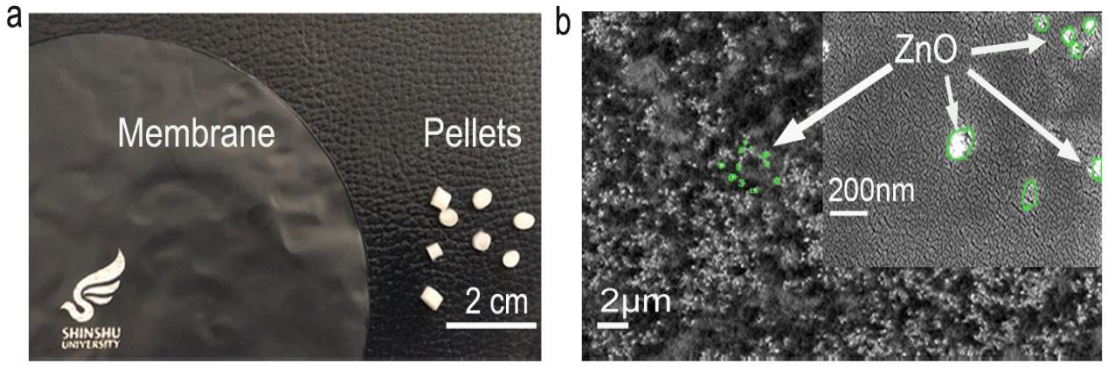

Fig. 4-7. a) Photographs of ZnO-LDPE transparent film and corresponding pellets; b) SEM image of embedded 6% ZnO NPs.

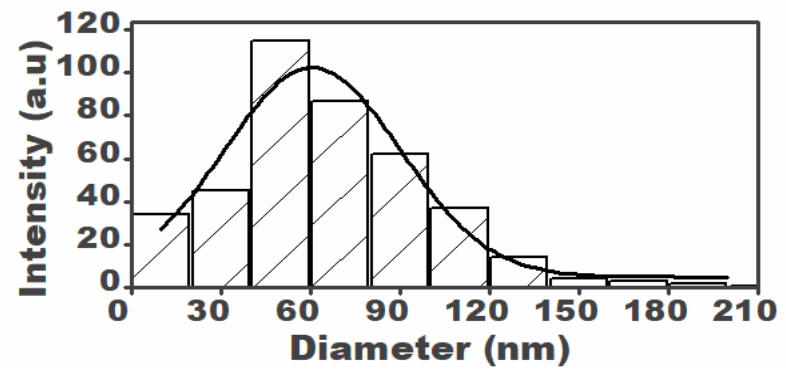

Fig. 4-8. Diameter distribution of ZnO NPs in the films.

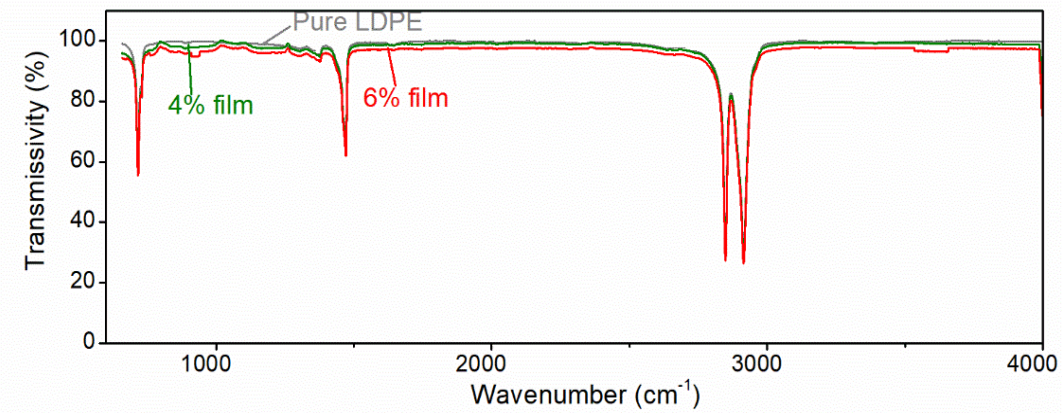

Fig. 4-9. Characteristic absorption peaks of pure LDPE, 4% film and 6% film in IR range.

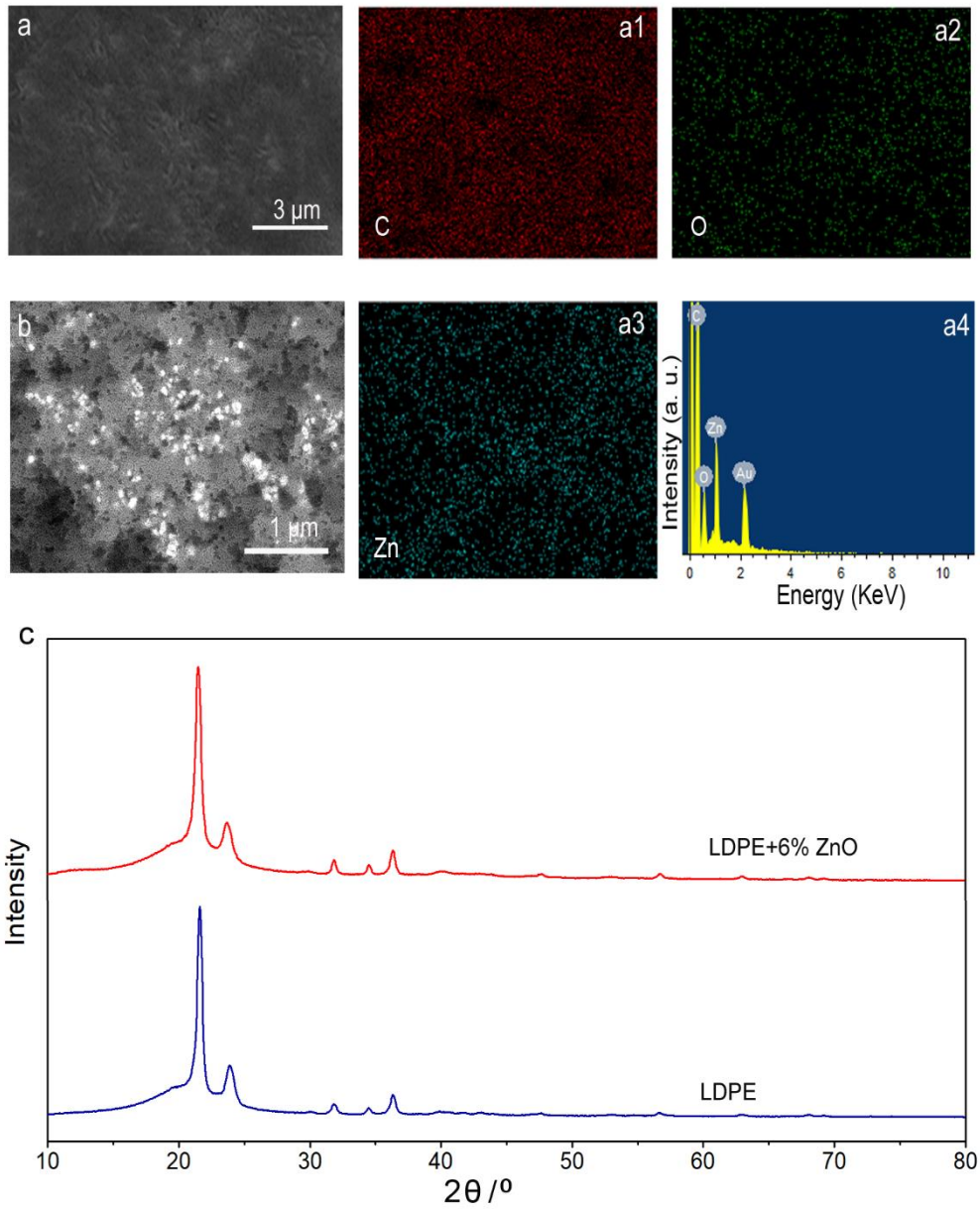

Fig. 4-10. SEM images and elemental analysis and mapping of the 6% ZnO/LDPE film. a) and b) SEM images with scale bars indicating 3 μm and 1 μm, respectively. a1-a3). EDX mapping, including a1) C, a2) O, a3) Zn and a4) elemental analysis of ZnO/LDPE film, in which Au was introduced by SEM sample preparation. c) XRD pattern of pure LDPE and the 6% ZnO/LDPE composite film.

4.3.2 Transmittance of the ZnO/LDPE films

The UV-Vis-nIR and FTIR spectra of the films with different particle concentrations, film thicknesses, and crystallinities are presented in Figs. 4-11. a-c. However, in the mid-IR range (2.5–16 μm), the films had high transmittances that were almost independent of particle concentration, film thickness, and crystallinity. Therefore, Figs. 4-11b and c only present transmissivities for the films in 200–2500 nm wavelength range, which is the range of the solar spectrum (AM 1.5). The UV-Vis-nIR spectra showed that UV radiation (200-400 nm) was blocked more than 97% while Vis-nIR (400–2500 nm) and mid-IR were less blocked. This is because the particle size parameter X varies from 1.41–0.707, corresponding to the 200–400 nm wavelength range of UV light, due to the strong scattering effect from the 90-nm NPs [31]. However, as the wavelength increases to the Vis-nIR and mid-IR range, the X value decreases rapidly, diminishing the Raleigh scattering effect. Therefore, most of the Vis-nIR and mid-IR region can transmit through the passive cooling film. In addition, in the Vis-nIR range, the transmittance of the films decreased as the concentration of NPs and the film thickness increased (Figs. 4-11 a and 4-11 b). This is because more particles lead to a greater scattering effect and a thicker film could absorb more energy of light [34]. As shown in Fig. 4-11c, the transmittance also decreased as crystallinity increased because the polymer crystalline phase has a different refractive index from that of the amorphous phase. Consequently, light traveling through boundaries between different phases is deflected and refracted, thus changing direction, losing intensity, and reducing light transmittance [34]. To promote transmittance of the films, crystal growth during the passive-cooling film production needs to be controlled [35]. A schematic illustration of the interaction mechanisms

between the film and the UV and high-energy region of Vis-nIR spectra are shown in Fig. 4-11d.

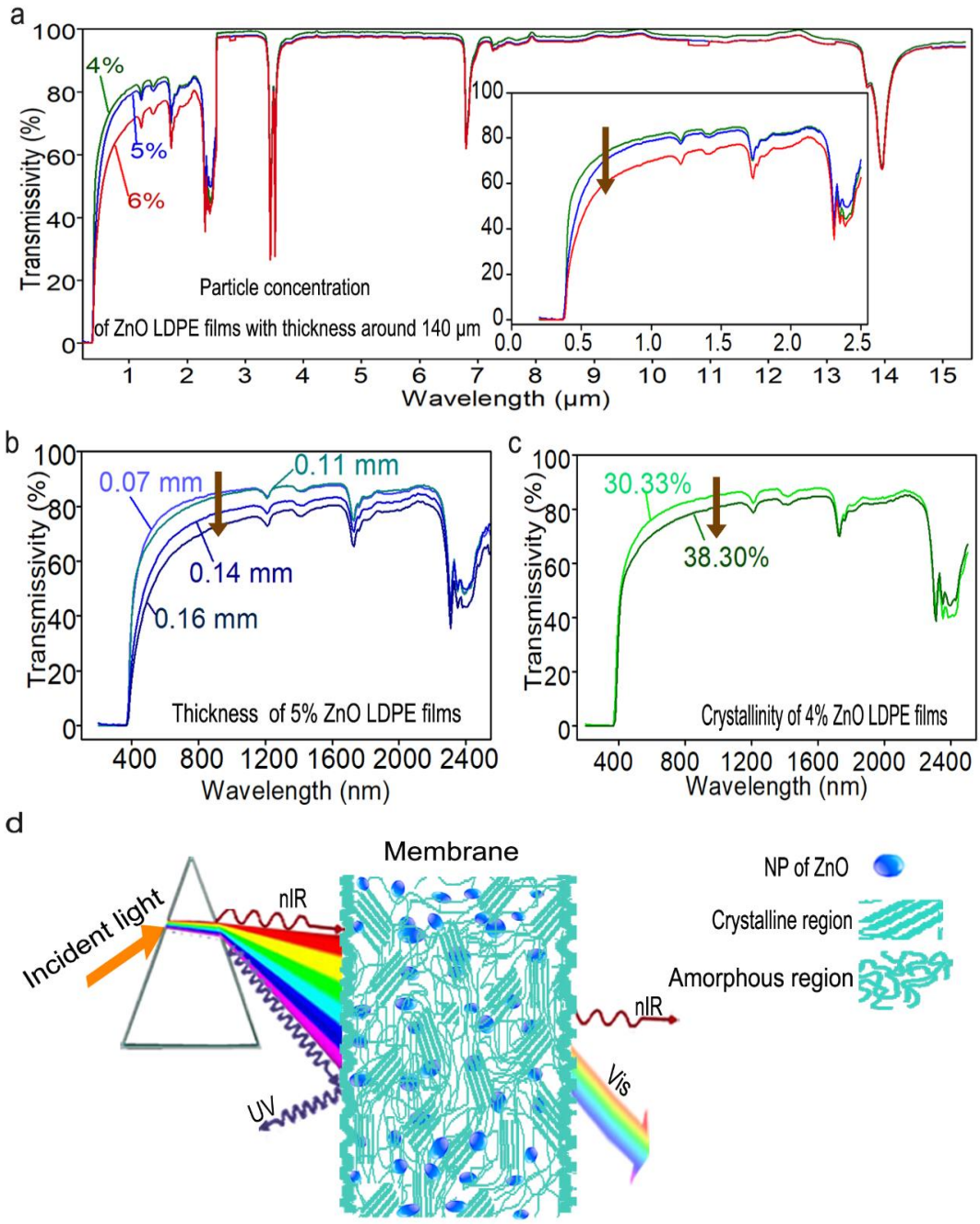

Fig. 4-11. a) Transmittances of three films with thicknesses around 140 μm containing different ZnO concentrations in thermal radiative wavelength range, b) Influence of film thickness on transmissivity of 5% ZnO PE films, c) Effect of crystallinity on

transmissivity of 4% ZnO LDPE films, d) Schematic illustration of nanostructure and shielding mechanisms for the semi-crystalline ZnO-LDPE films.

4.3.3 Solar spectrum monitoring and shielding function

The solar irradiance was monitored by PG2000-PRO (300 nm -1100 nm) and NIR2500 (900 nm- 2500 nm) during the testing passive cooling performances of spectrum selective materials**. Fig. 4-12**. b. shown the solar spectrum (AF 1.5) in per nano meter wavelength. The most intensity of solar radiation locates in the range of 400 nm to 1400 nm, and as the wavelength longer or shorter than the range, the irradiance is weaker relatively. The frequency of integration value data collection is 3 times per second. We selected 3 integration values per each 1 minute to show the solar radiation of one common day. And the solar integration values of one day showed in Fig. 4-12. a. from 10:30 to 16:00. It shows that the solar irradiation changes each second, and the trend of the strongest period of solar irradiance appears in the mid-day, around 12:00.

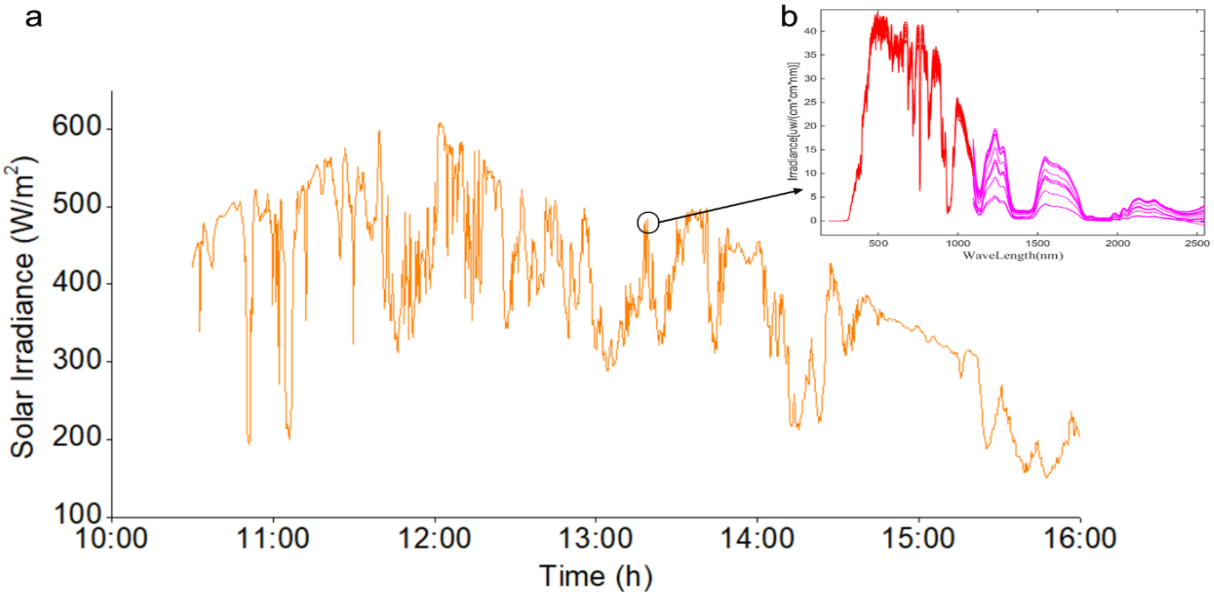

Fig. 4-12. Solar spectrum and integration solar irradiance of one common day.

The in-situ testing setup for passive cooling is shown in Fig. 4-5. c. The testing boxes were covered with a piece of glass (the control) or a piece of glass laminated with a ZnO/LDPE film with the similar thickness (0.14 mm) for particle concentrations of 4% and 6% named as 4% film and 6% film. The ZnO/LDPE spectrum selective films block UV and selectively reduce transmittance of Vis light, while allowing high passage of mid-IR (> 95% for both films) because of Mie and Rayleigh scattering as shown in **Fig. 4-13**. Solar irradiance at a certain moment and the shielding effect of the two films (4% film and 6% film) are presented in Fig. 4-13. The red curve is the transmissivity of 6 wt% ZnO/LDPE film, and the green one is the 4wt% ZnO/LDPE film. In which the light gray area is the solar radiation shielded by the 4% film, the light + dark gray area is that shielded by the 6% film, and the orange area is the transmitted solar irradiation through the 6%- film.

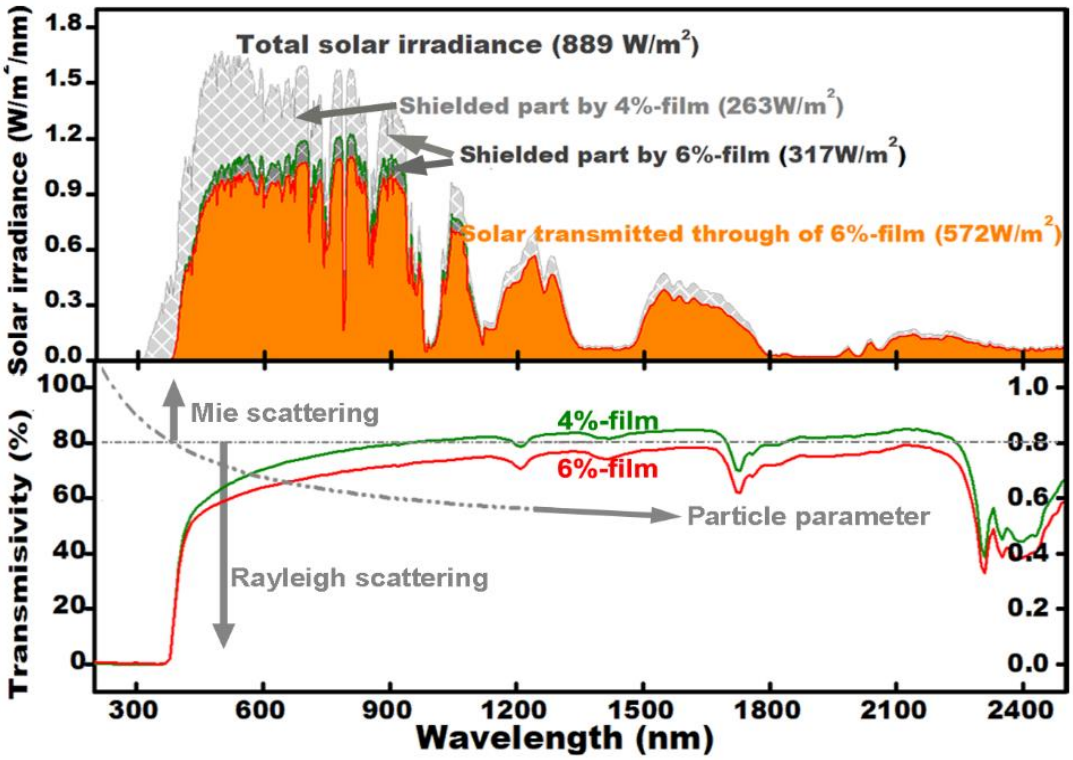

Fig. 4-13. Shielding portion of solar irradiance and transmissivity of 4% ZnO/LDPE film and 6% ZnO/LDPE film due to scattering mechanism of light travel through films.

4.3.4 Passive cooling performance

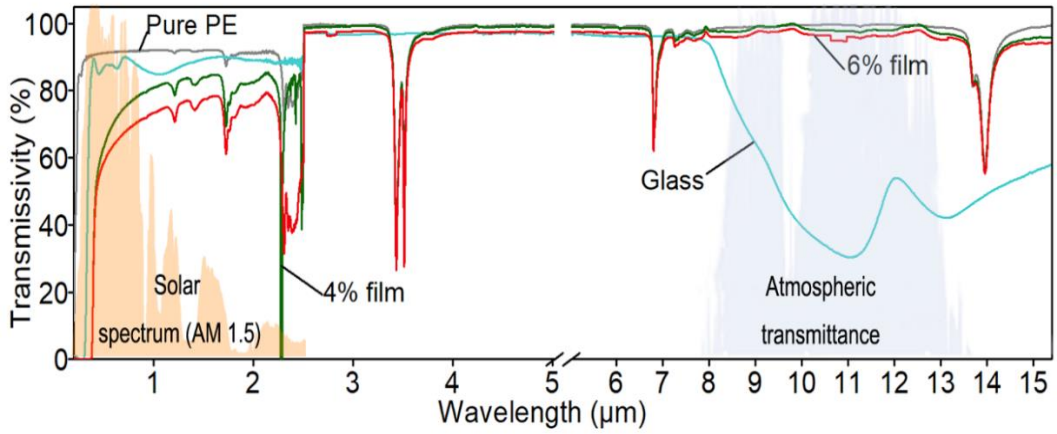

Fig. 4-14. Schematic of window's transmissivity of passive cooling testing facility

Glass has a transmittance more than 85% of solar irradiance but less than 40% transmissivity of near IR (9 – 14.5 μm) the blue line in **Fig. 4-14**. This ensures passage of higher energy photons while preventing mid-IR radiation going out. The window's spectrum transmissivity of the passive cooling testing facility showed in **Fig. 4-14.** The orange region is the solar irradiance spectrum of the earth surface (AM 1.5), and the blue region expresses the atmosphere window outer layer of earth.

The 24 h temperature monitoring results showed that the temperatures in the testing boxes were raised as the solar irradiation intensity increased **(Fig. 4-15**). At a fixed-box volume/window area of 1.92 m, the 4% film had the largest ΔT compared with the control at 12:28, reaching 4.86 ºC with a corresponding cooling power of 232 W/m^2 (A point and A' points in Fig. 4-15.), while that occurred for the 6% - film at 14:28, reaching 8.84 ºC, with a corresponding cooling power of 361 W/m^2 (B and B' points in Fig. 4-15.). It was also observed that the films had cooling effect at night, reaching 1.41 ºC at 1:15 (C point in Fig. 4-15.). It must be pointed out that the temperatures in all three boxes

were lower than the ambient temperature because thermal radiation from inside the box can be transmitted through the window, lowering the temperature inside the box.

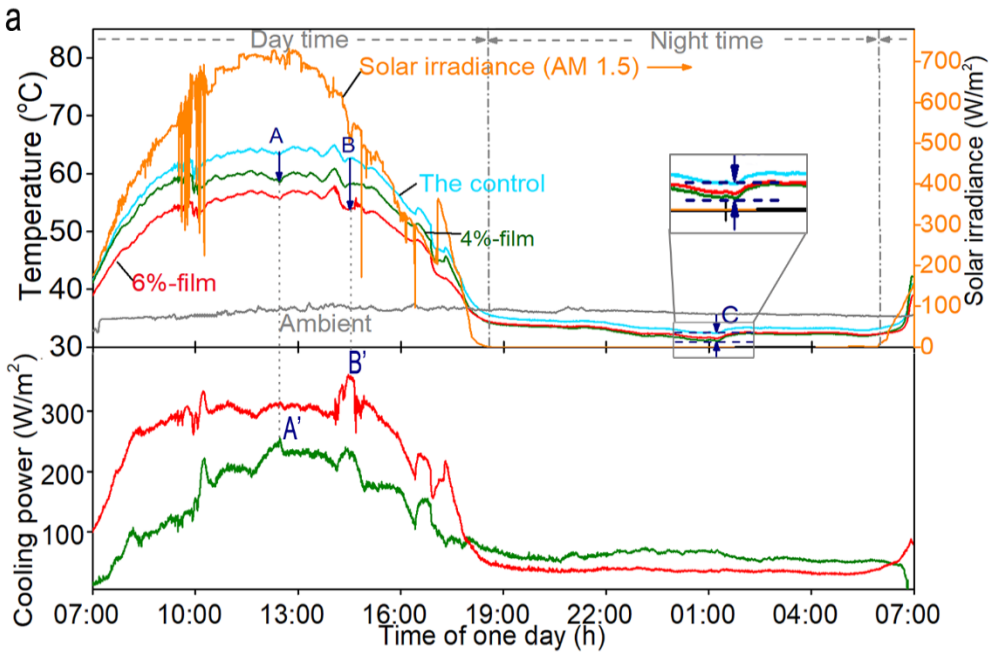

Fig. 4-15. In-box temperature variation for 24 h where maximum temperature reductions are marked by arrows. The 4% film and 6% film refer to 4 wt% and 6 wt% ZnO NPs in the films, respectively.

4.3.5 Specific volume effect on passive cooling performance

During our experiment, we found that the test box volume greatly influenced the cooling effect. We defined the ratio between the volume of the box V_b and the window size A_w to be the specific volume (SV):

$$\mathrm{SV} = \frac{V_b}{A_w} \quad \text{(m)} \qquad (4\text{-}7)$$

For the SV effect on cooling efficacy, the 6% film was tested using 9 SVs ranging from 0.06 to 21.83 m. For each SV, the film was tested 3 or 4 times from 10:30 to 16:00 to obtain an average value of ΔT. To generate a representative subset of the data for the volume effect, ΔTs were selected 10 min after solar irradiance reached 650 W/m^2.

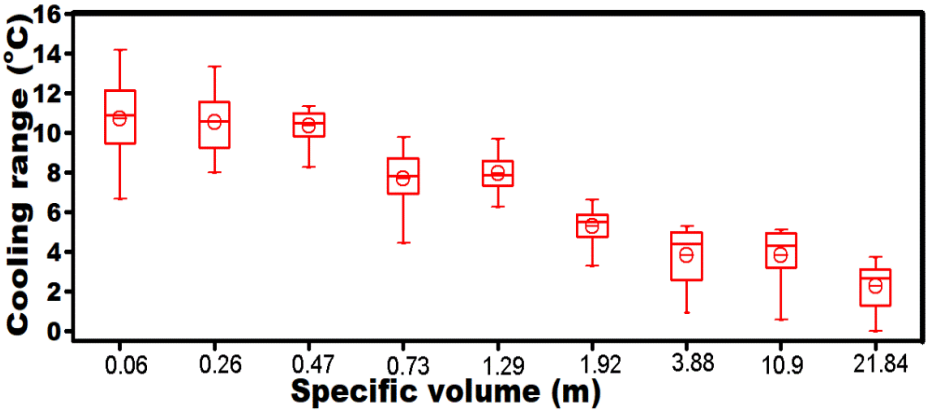

Fig. 4-16. Box plot for temperature reductions at different SV values, the lines in each box represent the maximum, 75, 50 and 25 percentiles from the top to the bottom, while the small square in the middle of each box refers to the mean.

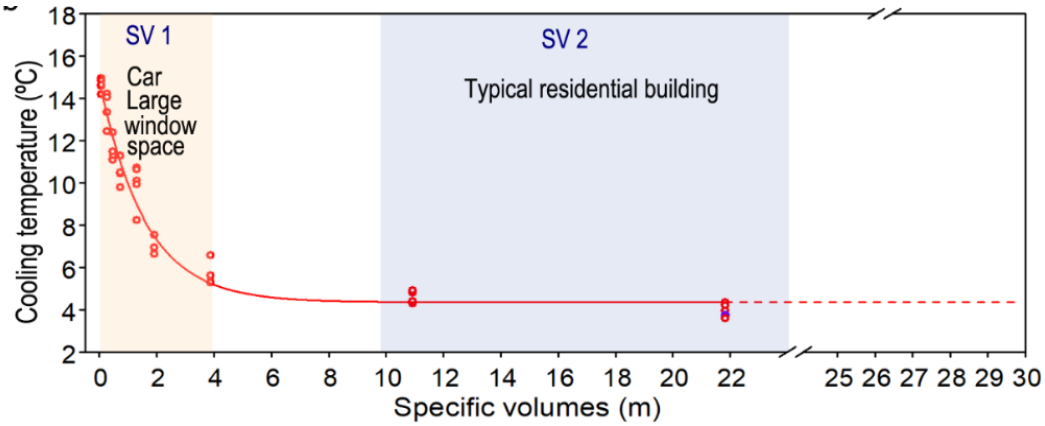

Fig. 4-17. Temperature reduction corresponding to the maximum solar irradiation as a function of SV.

Table 4-1. The maximum cooling performance of each SV

SV (m)	The maximum temperature reduction (°C)				
	1	2	3	4	Mean[d]
0.06	14.95[b]	14.79	14.84	—	14.86 ± 0.05
0.26	14.03	14.2	14.03	13.77	14.09 ± 0.09
0.47	12.37	11.00	11.11	11.58	11.49 ± 0.31
0.73	11.27	10.46	10.45	10.47	10.73 ± 0.20
1.29	10.62	10.11	10.72	9.93	10.48 ± 0.19
1.94	8.84[a]	7.82	7.51	6.94	8.06 ± 0.40
3.88	5.16	5.30	3.86	5.07	4.77 ± 0.33
10.93	5.06	4.87	3.93	—	4.61 ± 0.35
21.84	3.57	4.20	4.34[c]	4.03	4.04 ± 0.17

[a)] Data corresponding to B point in Fig. 4-9;

[b] Maximum temperature reduction at SV = 0.06;

[c] Maximum temperature reduction at SV = 21.84;

[d] Mean ± standard errors of mean.

As shown in **Fig. 4-16** and **Table 4-1**, ΔT increased from 4.34 to 14.95 ºC as SV decreased from 21 to 0.06 m. To study ΔT as a function of SV, a regression analysis was carried out as shown in **Fig. 4-17.** (R^2 = 0.96):

$$\Delta T = 4.35 + 10.50 \exp\left(-\frac{SV}{1.58}\right) \quad (4\text{-}8)$$

When SV → 0, ΔT reached the upper bound, ΔT_0 = 14.85ºC, which may be considered the intrinsic maximum temperature reduction of the film. As SV → ∞, ΔT approached the lower bound, ΔT_∞ = 4.35ºC. In general, when SV > 4.00 m, cooling effect levels off. The constant 1.58 m represents how quickly ΔT reduces as SV increases, which may be called cooling effect diminishing parameter, D. The above empirical model can be written as:

$$\Delta T = \Delta T_\infty + (\Delta T_0 - \Delta T_\infty) exp\left(-\frac{SV}{D}\right) \quad (4\text{-}9)$$

A larger D value means a slower declining of cooling effect as SV increases. The range of ΔT, ΔT_0 - ΔT_∞, is rather similar to what has been reported in the literature for solar control films in buildings and smart windows for automobiles. Zhu and coworkers [2] used multilayer emitters for day-time radiative cooling and observed ΔT of 9 – 12 ºC for SV around 0.02 m, somewhat lower than $\Delta T_{SV=0.02}$ = 14.72 ºC calculated Equation 3 in the current study. Likewise, other studies reported similar results. For instance, Zhang

et. al. [3] and Kou and coworkers [4] reported ΔT values close to our model prediction shown as the blue triangles in Fig 4-11 with SV values from 0.04 to 0.70 m. Raman et al [5] and Fan et al [6] reported that their photonic radiative coolers were able to reduce temperature by 4.9 ºC and 4.6 ºC, respectively, below ambient temperature in an open space set up in which SV → ∞, close to ΔT_{∞} = 4.19 ºC in the current study. Therefore, one may consider ΔT_{∞} as how much the film can passively reduce temperature below ambient temperature in an open space [7]. Since our test was carried out in a sealed box without the influence of surrounding heat transfer from thermal convection and irradiation, it could more accurately represent the performance of the film than the type of open frame tests reported in literature [5, 7].

Perhaps it is also important for us is to compare the results of the current study with intended end uses of the films. It is estimated that the SV values for passenger cars and office offices with large windows are around 0.05 – 3.5 m, well located in the range of rapid declining section of the ΔT vs SV curve as marked SV1 in the shaded areas in Fig. 4-11. For some residential buildings, SVs could be about 9.5 – 32.3 m (marked as SV2) at which ΔT is not so sensitive to SV change. Therefore, the cooling film can be highly beneficial for energy saving of passenger cars and large window offices that have relatively small SVs. Meanwhile, even for regular residential buildings and open spaces, the film could potentially lower the temperature by about 4 ºC in the mid-day, significantly reducing cooling energy consumption.

4.3.6 Effect of nanoparticle concentration on passive cooling performance

Three films with ZnO NP concentration of 4, 5, and 6 wt%, respectively were tested the cooling function. The particles shown in these images are clearly identifiable and well dispersed. The elemental analyses of three films show that films are composed of carbon, oxygen, and zinc, from the raw materials of LDPE and ZnO, and gold from the coating on surface of the SEM specimens.

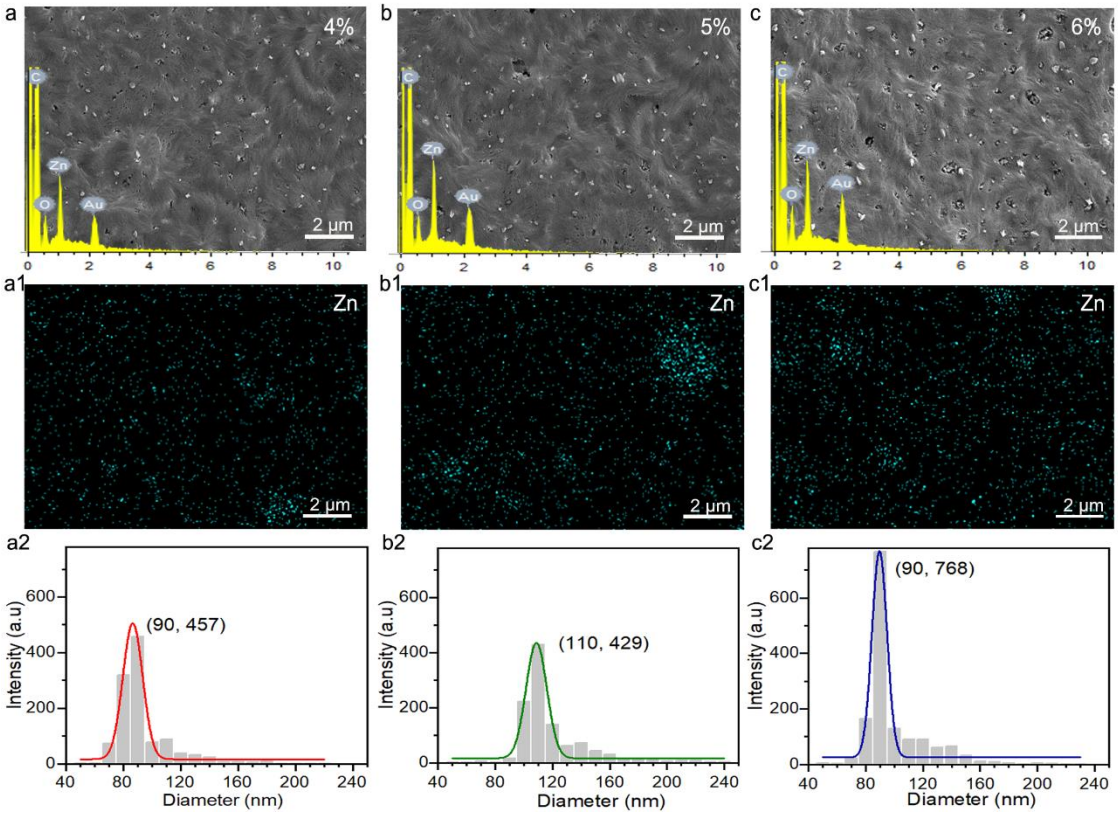

Fig. 4-18. SEM images of surface morphology and NP dispersion of ZnO/LDPE spectrum tailoring films with different ZnO concentrations: a), b), and c) SEM images; a1), b1), and c1) EDX mappings of Zinc element; a2), b2), and c2) NP diameter distributions corresponding to 4%, 5%, and 6% ZnO/LDPE films.

The dispersion of NPs of ZnO/LDPE is truly critical for spectrum selective function of these kind of membranes, the EDX mappings of Zinc element (a1, b1, and c1 in Figure 3), corresponding to samples of 4%, 5%, and 6%, show that the ZnO NPs were well dispersed in the films. The diameters of NPs were in the range of 20 nm to 220 nm, with the distribution of the NP diameters obeyed the Gaussian dispersion model, where the peaks of them were all around 90 nm.

The fractional distribution of an incident electromagnetic spectrum on a translucent film can be expressed as follows:

$$\alpha + \rho + \tau = 1 \qquad (4\text{-}10)$$

where α is the fraction of absorptance which is absorbed into the film; ρ is the reflectance representing the part of the incident spectrum reflected from the film surface; and τ is the transmittance, which is the light passes through the film. This means that the extinction part of the incident light is either reflected or absorbed by the film. The transmissivities, absorptivities, and reflectivities of the three spectrum selective films and the pure LDPE film were shown in **Fig. 4-19**. Compared with the pure LDPE film, the transmittances of the NP doped films were substantially decreased, especially in the two regions of incident light (200 - 400 nm and 2200 - 2500 nm) where the transmissivities were sharply reduced (shown in Fig.4-19 a). The absorptivities of the doped films were lower than 3% in region of 200 to 2500 nm (shown in Fig.4-19. b and c). The reflectivity curves of the three NP composite films had the opposite trend to those of the transmittivity curves. Obviously, the extinction part of the incident beam was mainly shielded by scattering or reflection of the films due to existence of the well dispersed NPs. Among the films with different NP concentrations, the 4% film had the highest transmissivity while the 6% film had the lowest in the high energy region of the

Vis light and intermediate transmissivity in the lower energy range of Vis and nIR region. This is rather ideal since it is preferred to block high energy part of the solar irradiation while allowing transmission of the lower energy part of the light, facilitating IR radiation from the heated body. Therefore the 6% film seems to have performance in this study.

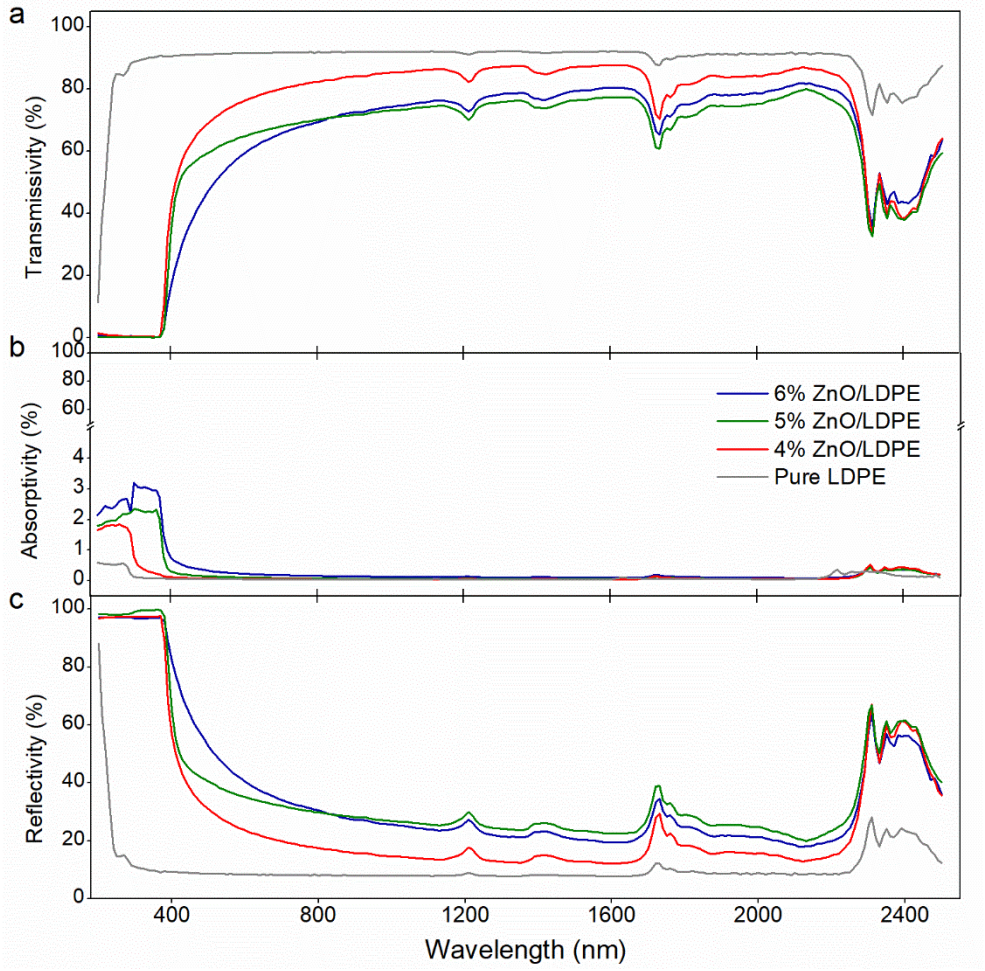

Fig. 4-19 The optical characters of the spectrum tailoring films. a). the transmissivity, b). the absorptivity, and c). the reflectivity curves in wavelength range of 200 nm to 2500 nm where gray, red, green, and blue corresponding to the pure film, 4%, 5%, and 6% ZnO/LDPE films, respectively.

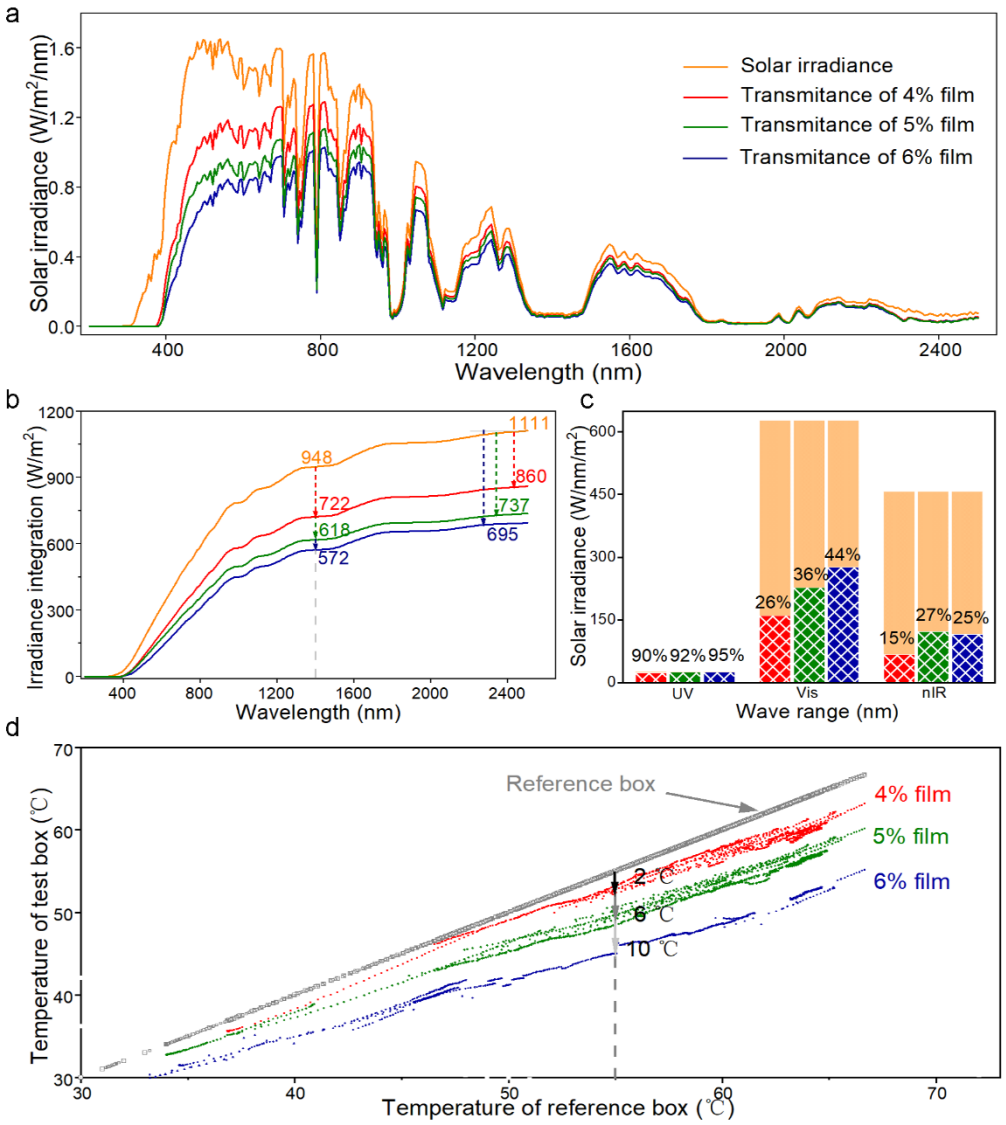

Fig. 4-20. Performances of solar irradiance shielding and passive cooling of 4%, 5%, and 6% ZnO/LDPE films. a). Transmission of solar irradiance for ZnO/LDPE films; b). The integration of transmission of solar irradiance of corresponding ZnO/LDPE films; c). Fractions of shielded solar irradiance (the grides filled in red, green, and blue are the shielded parts by 4%, 5%, and 6% ZnO/LDPE films in UV, Vis, and Nir region, respectively); d). Comparison of temperatures in shielded boxes and the control box.

The distributions of transmitted light and integrations of solar irradiance passed through the window of the test boxes are showed in **Fig. 4-20**. a and b. The shielding fractions of solar irradiance are showed in the Fig. 4-20. c. And the reflectance of 0%, 4%, 5%, and 6% NP doped film corresponding to UV, Vis, nIR and total solar spectrum regions are shown in the Table 1. The solar spectrum reflectance ($R_{(\lambda)}$) for each wavelength range can be determined as follows:

$$R_{(\lambda)} = \frac{\int_{\lambda_1}^{\lambda_2} i(\lambda)d\lambda - \int_{\lambda_1}^{\lambda_2} \alpha(\lambda)d\lambda - \int_{\lambda_1}^{\lambda_2} \tau(\lambda)d\lambda}{\int_{\lambda_1}^{\lambda_2} i(\lambda)d\lambda} \times 100\% \qquad (4\text{-}9)$$

where, $i(\lambda)$ is the intensity of solar irradiance; $\alpha(\lambda)$ is the intensity absorbed by film; $\tau(\lambda)$ is the intensity of the solar irradiance passed through the film. As shown in Table 1, R_s, R_{UV}, R_{Vis} and R_{nIR} are the reflectances of the materials in total solar spectrum, UV (200-400 nm), Vis (400-800 nm), and nIR (800-2500 nm) region, respectively. $R_{(\lambda)/T}$ is the reflectance corresponding to a certain wavelength range as a fraction of total solar irradiation spectrum calculated as:

$$R_{(\lambda)/T} = \frac{\int_{\lambda_1}^{\lambda_2} i(\lambda)d\lambda - \int_{\lambda_1}^{\lambda_2} \alpha(\lambda)d\lambda - \int_{\lambda_1}^{\lambda_2} \tau(\lambda)d\lambda}{\int_{200nm}^{2500nm} i(\lambda)d\lambda} \times 100\% \qquad (4\text{-}10)$$

The UV shielding performances of 4%, 5%, and 6% films are all over than 90% and the shielding percentage increases monotonically as the NP concentration increases. The same trend is observed for Vis lights. In nIR range, however, the 6% film had a smaller reflection than the 5% film. This can be explained by the dispersion of the NPs in the two films. In Fig. 4-18 b2 and c2, it can be seen that 6% film had a much more uniform NP distribution than that of 5% film where certain degree of NP agglomeration can

clearly be observed. This kind of agglomeration was not able to change reflectance in short wavelength but more influential for long wavelength range of solar irradiation since it is a long-range phenomenon. Obviously, the 6% film is more ideal since it reflects more high energy solar irradiance and less low energy Vis and nIR lights. Therefore, for this kind of NP doped composite films, it is important to have not only a reasonable NP concentration but also a uniform dispersion to achieve the best spectrum selective performance.

The temperature distributions of the tested boxes are showed in the Fig. 4-20. d. It indicates that as the accumulation of solar energy input into the test boxes, the temperature in the boxes steadily increased. The gray dot line showed the air temperature in the control box, and the red, green, and blue dot lines were the air temperature in the boxes covered with 4%, 5%, and 6% ZnO/LDPE films, respectively. When the air temperature of the reference box was 55℃, the air temperature of other boxes lined by 4%, 5%, and 6% ZnO/LDPE film was lower than that 2, 6, and 10℃, respectively. Regression analyses were carried out to access the passive cooling performance of the NP doped films. Table 2 shows the slopes of the fitted lines to the data in Figure 6 d. In fact, the slopes represent the average portion of temperature retention or 1 – temperature reduction.

Table 4-2. modulus of cooling regression equations

Samples	Fitted line slope	Temperature reduction (%)	R^2
4%	0.81	19	0.98
5%	0.79	21	0.99
6%	0.65	35	0.99

From Table 4-2, we are able to tell that the 4% and 5% films had almost the same

temperature reduction amount (19 and 21 %), while the 6% film had a greatly increased temperature reduction (35%). This again proved that good dispersion of NPs is much more important than simply increase the concentration of NPs. The reason for 6% film to have such a good performance is because it has best shielding against UV and high energy Vis but relatively low shielding against nIR, allowing heated box to emit nIR for temperature reduction.

4.3.7 Mechanical and thermal properties

The stress-strain curves of the three films are presented in **Fig. 4-21**. The ultimate strains of the ZnO/LDPE films decreased from 330% to 15% with the increase of NP concentration from 0 to 6 % although their yield strains are all around 10 – 15%. On the other hand, the tensile strength increased with the increase concentration of NP as reported in the literature [29, 30]. It seems that the mechanical properties of the films changed from being typical flexible materials to relatively brittle materials due to failure mechanism change from localized plastic deformation to more defect-dominant failure.

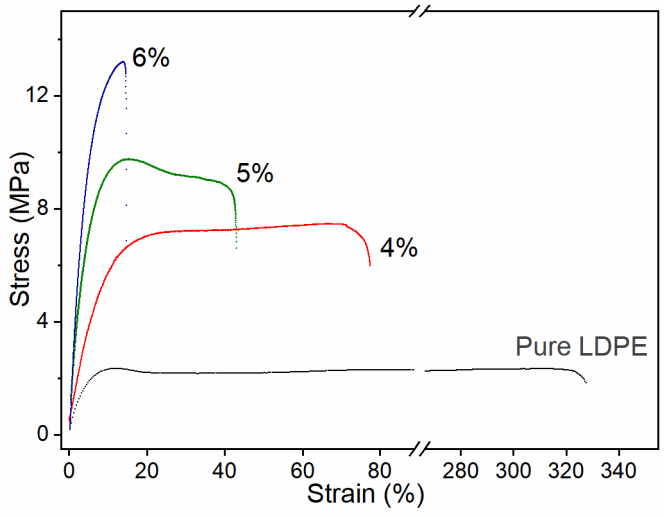

Fig. 4-21. The stress–strain curves of the films doped with different concentrations of

pure LDPE, 4%, 5%, and 6% of ZnO NP in LDPE.

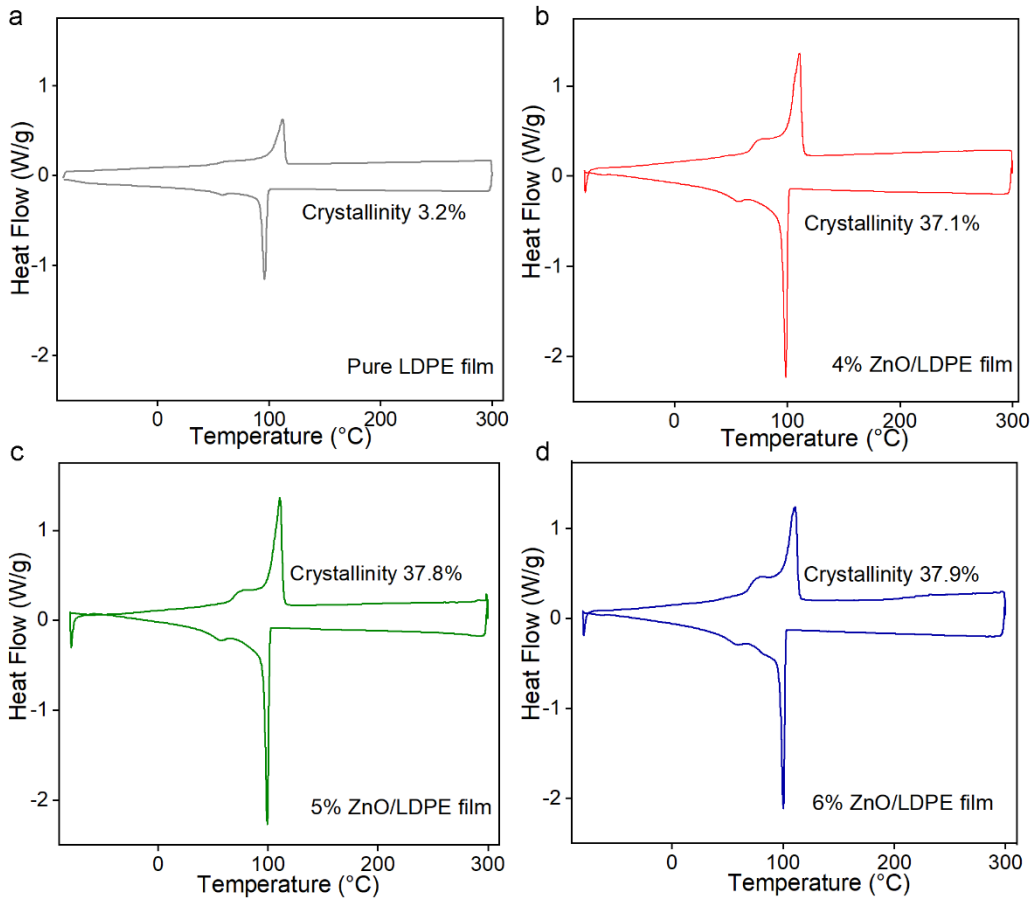

Fig. 4-22. a. Stress-strain curve of 6% ZnO-LDPE film; b. DSC curve of 6% ZnO-LDPE film.

The thermal properties of pure LDPE, 4%, 5%, and 6% of the spectrum selective ZnO/LDPE films were shown in Figure 4. Curves in gray, red, green, and blue displayed the first cycle of temperature change (increasing from -80 to 300 °C and then decreasing from 300 to -80 °C) at 10 °C/min. The crystallinity of pure LDPE film was 3.2%. The corresponding crystallinities were virtually the same for the three samples, namely 37.3%, 37.8%, and 37.9%, respectively.

The spectrum selective films have NPs, crystalline and amorphous phases of LDPE, resulting in plenty of boundary surfaces. When incident lights hit the films, only small

amount of light reflected on the film surface, while most of the lights were reflected and refracted when encountering the boundary surface, due to refractive index change of the different phases. However, if the crystallinities of the films are rather similar, the effect of crystallinity on shielding performance should also be similar for all films regardless the NP concentration. Therefore, the difference in shielding performance of the films created by different NP concentrations should mainly come from the NPs induced scattering.

4.4 Conclusions

In summary, transparent passive cooling films were manufactured using 90 nm ZnO NPs dispersed in LDPE. The films can almost completely shield UV and partially shield visible light due mainly to Rayleigh scattering while allowing most of IR to pass. The films were able to lower the temperature by 3.57 – 14.95 °C and the largest ΔT came with the smallest SV when solar radiation was the strongest during mid-day. An empirical model was derived between ΔT and SV, indicating that the cooling effect declines exponentially as the SV increases. As the SV approaches infinity, the ΔT remains as a constant around 4 ºC. The most effective range of the SV covers passenger cars and large window office buildings, indicating a great potential to use the film for energy saving for such applications. The films also have reasonable mechanical the thermal properties.

References

[1] R. Ruparathna, K. Hewage, R. Sadiq, Improving the energy efficiency of the existing building stock: A critical review of commercial and institutional buildings, Renew. Sust. Energ. Rev. 53 (2016) 1032-1045. https://doi.10.1016/j.rser.2015.09.084.

[2] R. Tällberg, B.P. Jelle, R. Loonen, T. Gao, M. Hamdy, Comparison of the energy saving potential of adaptive and controllable smart windows: A state-of-the-art review and simulation studies of thermochromic, photochromic and electrochromic technologies, Sol. Energy Mater. Sol. Cells 200 (2019) 109828-109858. https://doi.10.1016/j.solmat.2019.02.041.

[3] P.H. Shaikh, N.B.M. Nor, P. Nallagownden, I. Elamvazuthi, T. Ibrahim, A review on optimized control systems for building energy and comfort management of smart sustainable buildings, Renew. Sust. Energ. Rev. 34 (2014) 409-429. https://doi.10.1016/j.rser.2014.03.027.

[4] G.J. Marshall, C.P. Mahony, M.J. Rhodes, S.R. Daniewicz, N. Tsolas, S.M. Thompson, Thermal management of vehicle cabins, external surfaces, and onboard electronics: An overview, Engineering 5(5) (2019) 954-969. https://doi.10.1016/j.eng.2019.02.009.

[5] N. Gure, M. Yilmaz, Alternative solution via car window filming implementation to combat global warming and resulted benefits around geographic Europe and the European Union, Int. J. Glob. Warm. 10(1-3) (2016) 263-290. https://doi.10.1504/ijgw.2016.077917.

[6] I.E. Agency, Energy and air pollution World Energy Outlook Specoial Report,

https://webstore.iea.org/download/summary/343?fileName=English-WEO-Air-Pollution-ES.pdf, 2016 (accessed 3 July 2020).

[7] I.E. Agency, Energy in Buildings and Communities Annual Report https://www.iea-ebc.org/Data/Sites/1/media/docs/AR/ebc_annual_report_2018.pdf, 2018 (accessed 5 July 2020).

[8] N. Oreskes, The scientific consensus on climate change (vol 306, pg 1686, 2004), Sci 307(5708) (2005) 355-355. https://doi.10.1126/science.1103618.

[9] G.R. Walther, E. Post, P. Convey, A. Menzel, C. Parmesan, T.J.C. Beebee, J.M. Fromentin, O. Hoegh-Guldberg, F. Bairlein, Ecological responses to recent climate change, Nature 416(6879) (2002) 389-395. https://doi.10.1038/416389a.

[10] S.S. Chanisada Tuchinda, Henry W. Lim, Photoprotection by window glass, automobile glass, and sunglasses, J Am Acad Dermatol 54(5) (2006) 845-54. https://doi.10.1016/j.jaad.2006.05.014.

[11] R.V. Fahad Almutawa, Steven Q. Wang & Henry W. Lim, Current status of photoprotection by window glass, automobile glass, window films, and sunglasses, Photodermatology, Photoimmunology & Photomedicine 29(2) (2013) 65-72. https://doi.org/10.1111/phpp.12022.

[12] S. Li, J. Peng, Y. Tan, T. Ma, X. Li, B. Hao, Study of the application potential of photovoltaic direct-driven air conditioners in different climate zones, Energy Build 226 (2020) 110387-110400. https://doi.10.1016/j.enbuild.2020.110387.

[13] W. Li, S. Fan, Nanophotonic control of thermal radiation for energy applications Invited, Opt. Express 26(12) (2018) 15995-16021. https://doi.10.1364/oe.26.015995.

[14] J. Pereira, M. Gloria Gomes, A. Moret Rodrigues, M. Almeida, Thermal, luminous and energy performance of solar control films in single-glazed windows: Use of energy performance criteria to support decision making, Energy Build. 198 (2019) 431-443.

https://doi.10.1016/j.enbuild.2019.06.003.

[15] A.P. Raman, M.A. Anoma, L. Zhu, E. Rephaeli, S. Fan, Passive radiative cooling below ambient air temperature under direct sunlight, Nature 515(7528) (2014) 540-4. https://doi.10.1038/nature13883.

[16] T. Li, Y. Zhai, S. He, W. Gan, Z. Wei, M. Heidarinejad, D. Dalgo, R. Mi, X. Zhao, J. Song, J. Dai, C. Chen, A. Aili, A. Vellore, A. Martini, R. Yang, J. Srebric, X. Yi, L. Hu, A radiative cooling structural material, Sci 364(6442) (2019) 763- 760. https://doi.10.1126/science.aau9101.

[17] L. Cai, A.Y. Song, W. Li, P.-C. Hsu, D. Lin, P.B. Catrysse, Y. Liu, Y. Peng, J. Chen, H. Wang, J. Xu, A. Yang, S. Fan, Y. Cui, Spectrally selective nanocomposite textile for outdoor personal cooling, Adv. Mater. 30(35) (2018) 2152-2159. https://doi.10.1002/adma.201802152.

[18] E. Rephaeli, A. Raman, S. Fan, Ultrabroadband photonic structures to achieve high-performance daytime radiative cooling, Nano Lett. 13(4) (2013) 1457-1461. https://doi.10.1021/nl4004283.

[19] J.K. Tong, X. Huang, S.V. Boriskina, J. Loomis, Y. Xu, G. Chen, Infrared-transparent visible-opaque fabrics for wearable personal thermal management, Acs Photonics 2(6) (2015) 769-778. https://doi.10.1021/acsphotonics.5b00140.

[20] D. Fan, H. Sun, Q. Li, Thermal control properties of radiative cooling foil based on transparent fluorinated polyimide, Sol. Energy Mater. Sol. Cells 195 (2019) 250-257. https://doi.10.1016/j.solmat.2019.03.019.

[21] B. Xiang, X. Yin, J. Zhang, A novel cool material: ASA (acrylonitrile-styrene-acrylate) matrix composites with solar reflective inorganic particles, Compos. Sci. Technol. 145 (2017) 149-156. https://doi.10.1016/j.compscitech.2017.04.007.

[22] T. Li, Y. Zhai, S. He, W. Gan, Z. Wei, M. Heidarinejad, D. Dalgo, R. Mi, X. Zhao,

J. Song, J. Dai, C. Chen, A. Aili, A. Vellore, A. Martini, R. Yang, J. Srebric, X. Yin, L. Hu, A radiative cooling structural material, Sci 364(6442) (2019) 760-+. https://doi.10.1126/science.aau9101.

[23] J.V. Gulmine, P.R. Janissek, H.M. Heise, L. Akcelrud, Polyethylene characterization by FTIR, Polym. Test. 21(5) (2002) 557-563. https://doi.10.1016/s0142-9418(01)00124-6.

[24] W. Bond, Measurement of the refractive indices of several crystals, J. Appl. Phys. 36(5) (1965) 1674-1677. https://doi..org/10.1063/1.1703106.

[25] A.T. Young, Rayleigh scattering, Appl. Opt. 20(4) (1981) 533-535. https://doi.10.1364/ao.20.000533.

[26] A.H. Hsieh, D.S. Corti, E.I. Franses, Rayleigh and Rayleigh-Debye-Gans light scattering intensities and spetroturbidimetry of dispersions of unilamellar vesicles and multilamellar liposomes, J. Colloid Interface Sci. 578 (2020) 471-483. https://doi.10.1016/j.jcis.2020.05.085.

[27] M. Tasdemir, S. Ersoy, The mechanical and morphological properties of hdpe composites filled with sio2, zno, mg(oh)(2) and caco3 nano powder, Rev. Rom. Mater. 43(4) (2013) 417-424.

[28] J. He, W. Shao, L. Zhang, C. Deng, C. Li, Crystallization behavior and UV-protection property of PET-ZnO nanocomposites prepared by in situ polymerization, J. Appl. Polym. Sci. 114(2) (2009) 1303-1311. https://doi.10.1002/app.30614.

[29] R.E. Hummel, Part III Optical Properties of Materials, in: 4th (Ed.), Electronic Properties of Materials, Springer, New York, 2012, pp. 215-335.

[30] Y. Lin, R. Patel, J. Can, W. Tu, H. Zhang, E. Bilotti, C.W.M. Bastiaansen, T. Peijs, Glass-like transparent high strength polyethylene films by tuning drawing temperature, Poly 171 (2019) 180-191. https://doi.10.1016/j.polymer.2019.03.036.

[31] Y. Zhu, D. Wang, C. Fang, P. He, Y.-H. Ye, A multilayer emitter close to ideal solar reflectance for efficient daytime radiative cooling, Polymers 11(7) (2019) 1203-1213. https://doi.10.3390/polym11071203.

[32] H. Zhang, K.C.S. Ly, X. Liu, Z. Chen, M. Yan, Z. Wu, X. Wang, Y. Zheng, H. Zhou, T. Fan, Biologically inspired flexible photonic films for efficient passive radiative cooling, Proc Natl Acad Sci U S A (2020). https://doi.10.1073/pnas.2001802117.

[33] J.-l. Kou, Z. Jurado, Z. Chen, S. Fan, A.J. Minnich, Daytime Radiative Cooling Using Near-Black Infrared Emitters, ACS Photonics 4(3) (2017) 626-630. https://doi.10.1021/acsphotonics.6b00991.

[34] B. Zhao, X. Ao, N. Chen, Q. Xuan, M. Hu, G. Pei, General strategy of passive sub-ambient daytime radiative cooling, Sol. Energy Mater. Sol. Cells 199 (2019) 108-113. https://doi.10.1016/j.solmat.2019.04.028

Chapter 5 General conclusion

Chapter 5 General conclusion

We succeed developing a kind of spectrum selective nano composite films, which can almost shielding total of UV light and partial of Vis light, conversely, almost let the mid-IR trans through freely.

To make a spectrum selective or UV-shielding ZnO NP-doped film with uniform dispersion of the NPs and ideal transmissivity for spectrum tailoring, a systematic study was conducted to determine the critical parameters for film fabrication (e.g., casting temperature, polymer concentration, and dissolution time). It was found that the casting temperature has to be maintained at 115 °C or above in vacuum to ensure the formation of a transparent and uniform film without oxidation. For proper initial dispersion of the NPs in the polymer solution, the LDPE concentration should be lower than 6%. For a uniform and complete dispersion of individual NPs, the dissolution time has to be sufficiently long for the polymer molecules to unentangle first, which could allow the diffusion of the NPs into the polymer gel, thus resulting in a homogeneous NP dispersion. Only when the NPs are well dispersed will the film have ideal shielding against UV light while allowing a reasonable amount of visible light to be transmitted. The transmissivity of the films can be optimized by changing the concentration of doped NP and the crystallinity of the film through quenching. The mechanical properties of the UV-shielding films were altered from ductile to brittle by varying the NP concentrations.

Next, we selected different films and conditions to detect the cooling effects of our developed foils. And the corresponding factors are detected in detail, like the intensity of solar radiation, SV, and shielding ratio of Vis.

For detecting the intensity of solar radiation, we found that at a constant SV, the 4% - film had the largest ΔT compared with the control at 12:28, reaching 4.86 ºC with a corresponding cooling power of 232 W/m^2, while that occurred for the 6% - film at 14:28, reaching 8.84 ºC, with a corresponding cooling power of 361 W/m^2. It was also observed that the films had cooling effect at night, reaching 1.41 ºC at 1:15. It must be pointed out that the temperatures in all three boxes were lower than the ambient temperature because thermal radiation from inside the box can be transmitted through the window, lowering the temperature inside the box.

For the SV effect on cooling efficacy, the 6% - film was tested using 9 SVs ranging from 0.06 to 21.83 m. For each SV, the film was tested 3 or 4 times from 10:30 to 16:00 to obtain an average value of ΔT. ΔT increased from 4.34 to 14.95 ºC as SV decreased.

$$\Delta T = 4.35 + 10.50\exp\left(-\frac{SV}{1.58}\right) \qquad (5\text{-}1)$$

When SV → 0, ΔT reached the upper bound, ΔT_0 = 14.85ºC, which may be considered the intrinsic maximum temperature reduction of the film. As SV → ∞, ΔT approached the lower bound, ΔT_∞ = 4.35ºC. In general, when SV > 4.00 m, cooling effect levels off. The constant 1.58 m represents how quickly ΔT reduces as SV increases.

It is also important for us is to compare the results of the current study with intended end uses of the films. It is estimated that the SV values for passenger cars and office offices with large windows are around 0.05 – 3.5 m, well located in the range of rapid declining section of the ΔT vs SV curve as marked SV1 in the shaded areas in Fig. 4-11.

For some residential buildings, SVs could be about 9.5 – 32.3 m (marked as SV2) at which ΔT is not so sensitive to SV change. Therefore, the cooling film can be highly beneficial for energy saving of passenger cars and large window offices that have relatively small SVs. Meanwhile, even for regular residential buildings and open spaces, the film could potentially lower the temperature by about 4 ºC in the mid-day, significantly reducing cooling energy consumption.

We selected 3 passive cooling foils with different shielding ratio of Vis to monitor the passive cooling effect. the inner temperature of the reference box and the covered by cooling foil boxes, which was monitored from 10:30 to 16:00 of one day in early autumn. When the inner temperature of the reference box achieved to 55 ℃, the other boxes had 3 different cooling performance of 2 ℃, 6℃ and 10 ℃ lower than the reference boxes. The cooling performance was decided by the intrinsic transmissivity of each passive cooling films, also was influenced by the solar irradiance. The relationship between the shielding Vis ratio and cooling performance is liner ones.

In summary, transparent passive cooling films were manufactured using 90 nm ZnO NPs dispersed in LDPE. The films can almost completely shield UV and partially shield visible light due mainly to Rayleigh scattering while allowing most of IR to pass. The films were able to lower the temperature by 3.57 – 14.95 °C and the largest ΔT came with the smallest SV when solar radiation was the strongest during mid-day. An empirical model was derived between ΔT and SV, indicating that the cooling effect declines exponentially as the SV increases. As the SV approaches infinity, the ΔT remains as a constant around 4 ºC. The most effective range of the SV covers passenger cars and large window office buildings, indicating a great potential to use the film for

energy saving for such applications. The films also have reasonable mechanical the thermal properties.

List of publication

[1]. **Lina Cui**, Canyi Huang, Hong Xia, Yiping Qiu & Qing-Qing Ni,
Transparent Ultraviolet (UV)-Shielding Composite Films Made from Dispersing Virgin Inorganic Nanoparticles in Low-Density Polyethylene (LDPE),
Nanotechnology reviews, 9(1) (2020) 1368-1380.

[2]. **Lina Cui**, Canyi Huang, Hong Xia, Yiping Qiu & Qing-Qing Ni,
Transparent Passive Cooling Composite Films for Indoor and Outdoor Space,
Composites communications, 24 (2021) 100611-100617

Scientific presentation

International conference

1. **Lina Cui**, Canyi Huang, Hong Xia, Yiping Qiu & Qing-Qing Ni,
   Transparent Passive Cooling Composite Films for Indoor and Outdoor Space,
   Xiamen soft matter forum, 2019, Xiamen, China

Domestic conference

1. **Lina Cui**, Canyi Huang, Hong Xia, Yiping Qiu & Qing-Qing Ni,
   Transparent Passive Cooling Composite Films for Indoor and Outdoor Space,
   Symposium of advanced composites, 2019, Sapporo, Hokkaido, Japan

Acknowledgements

It is my great pleasure to work and do research with people who give me help and advice with no hesitate. Here, I want to give my best regards to all of you.

First, I want to give thanks to my supervisor, Prof. Qing-Qing Ni, who gives me the most important supports for my research work and encourages me to do some innovating work. He supervised me to overcome some critical encounters of my research. And guided me to be a qualified researcher. And he also carefully guided me about how to write scientific paper in a strict manner. Thanks to his guidance, because of his support I can defense my PhD in Shinshu University.

I want to express my thanks to Prof. Yiping Qiu (Quanzhou Normal University), Prof. Xiangyang Liu (Xiamen University), Prof. Shuiyuan Luo (Quanzhou Normal University), and Prof. Tingdi Liao (Quanzhou Normal University), thanks for their supporting works of my research.

I also want to express my thanks to Prof. Toshiaki Natsuki for his help for my research progress and living condition.

I need to express my wishes to researchers and technicians in our group, Hong Xia, Nakamura who gave me their help whenever I need, and assisted in experiments skills. As their help, I can make progress in my research quickly.

I want to express my gratitude to Interdisciplinary Graduate School of Science and

Technology (Shinshu University) for the financial support.

Thanks to all member of our group, for your introducing of different kinds of national cultures. And especially thanks to Hairong Chen, Juhong Yu, Xiaoyu Guan, Si Chen, Yajun Liu, Chongchao Li, Ran Li, Yongjie Yan, Jun Hong, Ke Ma, Jing Hui, Yinan Jing, Xiaojuan Li. Thanks for their help.

Finally, I need to thank my husband and my daughter. They always gave me their support in mental and living condition without any hesitated.